ABSTRACT

Title of thesis	Heat Transfer Coefficient and Pressure Drop Measurements for CO_2/Oil Mixture in a Micro Channel Tube
Degree Candidate	James Kalinger
Degree and Year	Master of Science, 2005
Thesis directed by	Professor Reinhard Radermacher, Ph.D. Department of Mechanical Engineering

An experimental study was conducted to measure the heat transfer characteristics and pressure drop of supercritical Carbon Dioxide (CO_2) in gas cooling conditions while flowing through a horizontal micro channel tube. Five experiments were conducted at operating conditions that included an inlet temperature of 70°, inlet pressures of 8 to 10 MPa, a mass flux of 400 kg/m^{2}s, heat fluxes of 10 and 15 kW/m^2, and oil concentration ratios of 6.58 to 10.72 wt.% with ND-8, polyalkylene glycol (PAG) oil. The main objective of the study was to determine how the oil concentration ratio (OCR) of this miscible oil affected the heat transfer coefficient of CO_2 and determine if there is a region of test conditions to target or avoid. The secondary goal of the study was to determine if the varying OCR amount also affected the pressure drop seen over the micro channel. Tests were performed using a micro channel that is 600 mm long and is made up of ten parallel circular ports that are 1 mm in diameter. Heat transfer was established by flowing water (H_2O) in a cross flow direction over the micro channel. The energy balance

originally produced error values of 50 to 60%, however after several alterations to both the H_2O and CO_2 side this was reduced to give errors of ± 8%. This data revealed trends that CO_2 flowing through a micro channel has a reduced heat transfer coefficient and an increased pressure drop with an OCR over 6 wt.% in comparison to the predicted values obtained from commonly used correlations. The measured heat transfer coefficient for the CO_2 was approximately 70% smaller than the predicted value using the Gnielinski correlation. The measured pressure drop for the CO_2 was approximately 150% larger than the predicted value using the Darcy-Weisbach correlation. Unfortunately, despite modifications the OCR level was never adequately controlled throughout the system thus preventing the test conditions that were specified to be completed.

HEAT TRANSFER COEFFICENT AND PRESSURE DROP GAS COOLING MEASUREMENTS FOR CO_2/OIL MIXTURE IN A MICRO CHANNEL TUBE

By

James Kalinger

Thesis submitted to the Faculty of the Graduate School of the
University of Maryland, College Park in partial fulfillment
of the requirements for the degree of
Master of Science
2005

Advisory Committee:

Professor Reinhard Radermacher, Ph.D., Chairman/Advisor
Professor David Bigio, Ph.D., Committee Member
Professor Linda Schmidt, Ph.D., Committee Member

Dedication

This is dedicated to those individuals who supported, encouraged and provided me with the faith to continue working when I was dejected; particularly my parents and my loving girlfriend, Lisa.

Acknowledgement

My thanks and gratitude goes to Dr. Reinhard Radermacher for giving me the opportunity to continue my education at the University of Maryland in the Center for Environmental Energy Engineering (CEEE) Department. Without his wisdom, encouragement, and advice this work would not have been completed. I would also like to say thanks to Dr. Yunho Hwang whose guidance was very beneficial.

I would like to particularly thank the past and present members of the CEEE Department. They provided me with knowledge, assistance in the lab, and were a great source of companionship throughout the endless hours of work we all dedicated. In the Heat Pump Lab these team members include: Lorenzo Cremaschi, Jan Muehlbauer, Amr Gado, Ahmet Ors, Jin Dae-Hyun, Mark Treadwell and Reni Muller. In the Compressor Lab these team members included John Linde, Alex Buchele and Xudong Wang. Again thank you and it was a pleasure working with each and every one of you.

I can not express in mere words the appreciation I have for my family members and my close friends. Both my parents and my sister were always there to say words of encouragement when I thought all hope was lost. Their constant support and love gave me the confidence and guidance to keep my head up and to continue trying.

I would like to acknowledge all the individuals I met at the University of Maryland who either aided me, made me a better person, or who just made me smile; particularly the advisors in the Mechanical Engineering Department and the QUEST Program.
Finally, I would like to say thank you to God. He is the reason so many blessed things have happened to me.

Table of Contents

List of Tables

List of Figures

List of Abbreviations

Symbol	Description	Unit
A	Area, surface	m^2
A	Wilson Plot constant (slope)	
AN	Alkyl Naphthalene Oil	
B	Wilson Plot constant (intersection)	
CEEE	Center for Environmental Energy Engineering	
CFC	Chlorofluorocarbons	
C_p	Specific Heat	J/(kg*K)
CO_2	Carbon Dioxide	
D	Diameter	m
D	Log. Wilson Plot constant (slope)	
E	Log. Wilson Plot constant (intersection)	
EES	Engineering Equation Solver	
f	Friction Factor	
g	Gravity	m/s^2
GWP	Global Warming Potential	
h	Enthalpy	kJ/kg
h	Heat Transfer Coefficient	$kW/(m^{2*}K)$
H_2O	Water	
HCFC	Hydrochlorofluorocarbons	
HFC	Hydrofluororcarbons	
k	Thermal Conductivity	kW/(m*K)
K	Minor Loss (pressure drop)	
L	Length	m
m	Mass Flow rate	kg/s
m	Mass Flux	$kg/(m^{2*}s)$
Nu	Nusselt Number	
OCR	Oil Concentration Ratio	%
ODP	Ozone Depletion Potential	

P	Pressure	MPa
PAG	Polyalkylene Glycol Oil	
PAO	Polyalphaolefin Oil	
Pr	Prandtl Number	
Q	Heat Transfer	kW
$\dot{Q}$	Heat Flux	kW/m^2
R	Thermal Resistance	$(m^2*K)/W$
Re	Reynolds Number	
T	Temperature	°C
θ	Theta	
U	Heat Transfer Coefficient	$kW/(m^2K)$
VCS	Vapor Compression System	
X_1	Independent Variable of Wilson Plot	
X_2	Independent Variable of log. Wilson Plot	
Y_1	Dependent Variable of Wilson Plot	
Y_2	Dependent Variable of log. Wilson Plot	
Δ	Difference	
ρ	Density	kg/m^3

Subscript	Description
a	Vertical Sides
amb	Ambient
b	Horizontal Sides
CO_2	Carbon Dioxide
h	Hydraulic
hi	Hydraulic Inside
ho	Hydraulic Outside
H_2O	Water

i	Inside
ins	Insulation
o	Outside
poly	Polycarbonate
w	Wall

1 Introduction

1.1 Overview

Environmental concerns of ozone depletion and global warming are impacting the refrigeration industry by means of new regulations that reduce or eliminate the use of current refrigerants. The 'Protocol on Substances that Deplete the Ozone Layer' of Montreal in 1987 initiated the phase out of chlorofluorocarbons (CFC) as a refrigerant in industrialized countries because of their high Global Warming Potential (GWP) and high Ozone Depletion Potential (ODP). At the present time, hydrochlorofluorocarbons (HCFC) are being used as a refrigerant because of their reduced ODP. However HCFC's are not an optimal choice because there still exists a limited ODP, a high GWP, and are a high cost. Another mandate in the Montreal Protocol is a ban on HCFC's by the year 2020; however some environmentally active countries have already reached this goal. Hydrofluorocarbons (HFC) were developed to replace both CFC's and HCFC's, but there is still concern about their behavior as a greenhouse gas in the atmosphere due to their high GWP. The Kyoto Protocol of 1997 called for reduction of greenhouse gases, including HFC's such as R-134a. (Rieberer)

In order to avoid the environmental problems of refrigerants such as CFC's and HCFC's, the industry looked toward 'natural' alternatives. Both Ammonia and Carbon Dioxide were implemented in the mid-1800's as natural refrigerants, although they were both phased out due to the dangers associated with their toxicity and high pressure operating conditions, respectively. Propane has also been suggested as a favorable natural refrigerant.

(Lorentzen) Table 1 shows basic characteristics of a CFC, HCFC, HFC and all three natural refrigerants just mentioned. It should be noted that the GWP for all six are measured in relation to CO_2 at 20 and 100 years integration. It is clear from the ODP and GWP values that the natural refrigerants have a distinct advantage in terms of being environmentally friendly. The benefit of CO_2 over Propane and Ammonia is that it is non-toxic, incombustible, has no ODP and negligible GWP. An additional advantage is that CO_2 is very inexpensive.

Table 1: Characteristics of Refrigerants (Lorentzen, 1995; VDI, 1994, FERRET)

Refrigerant	**R-12 (CFC)**	**R-22 (HCFC)**	**R-134a (HFC)**	**R-290 (Propane)**	**R-717 (Ammonia)**	**R-744 (Carbon Dioxide)**
Chemical Formula	CCl_2F_2	$CHClF_2$	CH_2FCF_3	C_3H_8	NH_3	CO_2
Natural	No	No	No	Yes	Yes	Yes
ODP	1	0.05	0	0	0	0
GWP[(a)] 100 20	7,100 7,100	1,500 4,100	1,200 3,100	3	0	1
Flammable	No	No[(b)]	No[(b)]	Yes	Yes	No
Toxic	Yes	Yes	Yes	No	No	No
T_{crit} [°C]	112.0	96.2	101.2	96.7	132.3	31.1
P_{crit} [bar]	41.6	49.9	40.7	42.4	113.3	73.8

[(a)]Global Warming Potential in relation to CO_2 with 20 and 100 years integration time.
[(b)]Usually considered non-flammable, both are combustible in certain mixtures with air at elevated pressures, but ignition may be difficult.

1.2 Motivation

Therefore, it is known that CO_2 has improved environmental impact characteristics compared to current refrigerants. The question remains, are its thermodynamic characteristics suitable to be used as an efficient refrigerant? Although the working pressure for CO_2 is considerably higher than the other refrigerants, its high heat transfer

characteristics and high volumetric capacity make it an excellent choice for a refrigerant. These attributes allow for compressors, piping and heat exchangers built for CO_2 to be smaller than those for the more common refrigerants, reducing the size of the entire refrigerant system. Certain applications that are considered favorable to use CO_2 as a refrigerant have been in heat pump water heaters, laundry dryers, mobile air conditioners and heat pumps. (Halozan) Since CO_2 can transport a high amount of heat in smaller devices, micro channel heat exchangers that have high pressure capability have been developed for use with CO_2. Micro channels have been widely used for heat exchangers because of their significant reduction in face area with air passing over them, in addition to their high heat transfer coefficients. The reduction in face area with air does not correlate to a decrease in heat transfer area; conversely, the heat transfer area is actually increased with the use of micro channels. CO_2 is advantageousfor use with micro channels because of its much smaller surface tension and viscosity compared to common refrigerants. These characteristics allow CO_2 to yield great results in extremely small hydraulic diameter sized tubing. (Petterson) Since micro channels have hydraulic diameters usually less than 1.5 mm, CO_2 is a desirable refrigerant to use.

1.3 Objective

There are several challenges to using CO_2 as a refrigerant. Most notably, new cycle apparatuses likecompressors and heat exchangers need to be designed to withstand CO_2's high operating pressure. Unfortunately, there has not been a fully comprehensive study on CO_2 as a refrigerant due to a lack of world wide acceptance. Those who have recognized

CO_2's potentialhave only done so in the past decade, providing a limited time to produce all of the data needed. (Halozan) The process of researching CO_2 refrigerant systems has already started and increased dramatically. Prototype compressors and heat exchangers that are currently being implemented with other refrigerants are altered to increase the efficiency by adhering to the thermal characteristics of CO_2. Some companies such as Coca-Cola have already introduced field tests with CO_2 by implementing it in some of their vending machines in Spain, Japan, Greece, and Australia. (Gabola)

The most significant disadvantage of the high operating pressure requirement is that in combination with the polarity of CO_2, lubrication of compressors can be more difficult. (Drees) This paper explores how the inclusion of oil in CO_2 can affect its thermodynamic characteristics. It is imperative to have oil in the system to prevent the compressor from overheating by lubricating its moving parts. However it is not known how the heat transfer characteristics and pressure drop in micro channel heat exchangers will be effected by the addition of oil circulating with the CO_2.

CO_2's use as a refrigerant has not been completely studied, thus the goal of this project is to observe a specific implementation of CO_2. The basis of this experiment is to evaluate the gas cooling heat transfer coefficients and the pressure drop for a flowing mixture of CO_2 and miscible oil in a micro channel under varying conditions. These results will then be compared to current correlations and past research result papers for accuracy. Finally, conclusions will be drawn on the effect of the OCR on CO_2 as a refrigerant. A wide range of experimental test conditions are defined in Table 2. These operating conditions include

altering the miscible Polyalkylene Glycol (PAG) oil concentrations from 0-5 wt.%, changing the mixture inlet pressure, temperature, mass flux and the heat flux along the test section itself.

Table 2: Gas Cooling Testing Conditions

Inlet Temperature (°C)	**Pressure (MPa)**	**Mass Flux (kg/m^2s)**	**Heat Flux (kW/m^2)**	**OCR (wt. %)**
70	8 10 12	400 600 800 1000	5 10 15	0 - 5
80				
90				
100				

The contribution of this project is to expand upon current reports results to obtain a better understanding of CO_2 and oil mixtures by first verifying the earlier data and then developing new conclusions from increased test conditions. It should be noted in this report only PAG oil will be tested since it is a miscible oil, unlike Alkyl Naphthalene (AN) and Polyalphaolefin (PAO) which are not miscible with CO_2.

2 Background

2.1 Literature Review

Experimental tests have been performed by Tran et al. (1996), Yang and Webb (1997) and others to show that CO_2 acts as theoretically predicted without oil circulating in a refrigerant cycle. Tran studied laminar and turbulent boiling heat transfer in small circular and rectangular channels, concluding that for wall superheats above 2.75 K nucleate boiling mechanisms dominate over forced convection. Yang and Webb compared their experimental results with commonly referred to correlations and found that Shah's (1979) correlation prediction over estimates the heat transfer co-efficient. Akers et al. (1959) correlation is reasonable for small mass fluxes. Additionally, Zhao et al. (1999) performed a study on convective boiling CO_2 in micro channels to determine heat transfer and pressure drop effects without the implement of oil circulation. They deduced that an increased mass flux did not affect the heat transfer co-efficient while drastically increasing the pressure drop over the micro channel. They also concluded that an increase in inlet CO_2 temperature decreased both the heat transfer coefficient and the pressure drop. Neksa et al. (2001) focused on the heat transfer and pressure drop for evaporating flows of CO_2 in aluminum micro channel tubes. They concluded that heat transfer coefficients up to 20-25 kW/m^2K could be expected in the nucleate boiling region. Additionally, they observed a critical heat flux phenomenon where there was a sudden decrease in the heat transfer coefficient at a certain vapor fraction and above if the CO_2 was flowing at a high mass flux.

Pettersen et al. (2000) performed similar tests in micro channel tubes, testing both supercritical and sub-critical CO_2, which refers to gas cooling and convective boiling, respectively. Their motivation was to obtain heat transfer and pressure drop data for heat exchangers used in the trans-critical CO_2 region and to compare this to common engineering correlations for this region. The experimental tests were conducted over a range of inlet pressures (8.1 to 10.1 MPa), temperatures (20 to 60°C), mass fluxes (600 to 1200 kg/m^{2}s) and heat fluxes (10 and 20 kW/m^2). With regard to the gas cooling conditions which this report focuses on, Petterson concluded that the Gnielinski correlation using the Haaland friction factor and considering the influence of the wall temperature was within -1% σ_{avg} of the measured heat transfer and that the Ghajar and Asadi (1986) correlation was within 1% σ_{avg} as well. Other correlations studied that produced much larger σ_{avg} were the Gnielinski using the Filonenko friction factor, the Polyakov and the Dittus-Boelter. The pressure drop was also measured and compared to conventional correlations, producing the results that both the Colebrook & White correlation and the Swamee correlation were accurate up to 1% σ_{avg}. As shown there is substantial research done in verifying and predicting the thermal characteristics of CO_2, however there is little data experimenting how various amounts of oil concentration ratios alter these characteristics.

One of the few CO_2 studies with OCR was undertaken by the Center for Environmental Energy Engineering (CEEE) at the University of Maryland by Kuang et al. (2004); but the test conditions which they implemented were restricted, only altering the values of the inlet temperature, the oil concentration ratio and the oil in which they mixed. They utilized

a circular port micro channel that had eleven ports of a diameter 0.79 mm. Their test conditions can be seen in Table 3.

Table 3: CEEE Previous Gas Cooling Test Conditions

Pressure (MPa)	Mass Flux (kg/m^2s)	Inlet Temp (°C)	OCR (wt. %)	Oil
9	844	25 – 50	0 - 5	PAG, POE, AN/PAG

This project will use the PAG oil used and the OCR amounts through the micro channel as was done in the Kuang et al. study. In addition the pressures, mass flux and heat flux will also be varied. This paper focuses on the temperature range of 70°C to 100°C, a more realistically observed range for CO_2 in gas cooling conditions. Kuang et al. focused on 25°C to 50°C to observe how the mixture reacted around CO_2's critical temperature, 31.1°C. They found that around 40°C there was a spike in heat transfer enhancement of approximately two and a half times when compared to the results found at 30°C for 0% OCR. However, a 3% increase in the OCR decreased this enhancement down to 1.4 times. Kuang et al. also deduced that an increase in OCR related to an increase in pressure drop over the micro channel. His findings will be discussed in more detail when compared with the data received for this project in the Discussion section. Kuang et al. provided a very interesting foundation in reference to the characteristics associated with oil circulating in CO_2, which this paper hopes to build upon.

3 Experimental System

3.1 Layout Overview

The first step of the project was to design the experimental facility system. A simple design was chosen that can be observed in Figure 1, in which there are two loops. The loop to the right consists of a Vapor Compression System (VCS) that includes a compressor, gas cooler, expansion valve 1 and an evaporator. The purpose of the VCS was to establish the test conditions listed in Table 2. Two oil separators are placed after the compressor to eliminate the circulation of oil throughout the entire system. The oil separators have a drain pipe that goes back to the suction of the compressor, refilling the oil back into the compressor. In addition, the oil separators can drain oil into the oil reservoir which will be mentioned in the next loop. There are pressure transducers, labeled

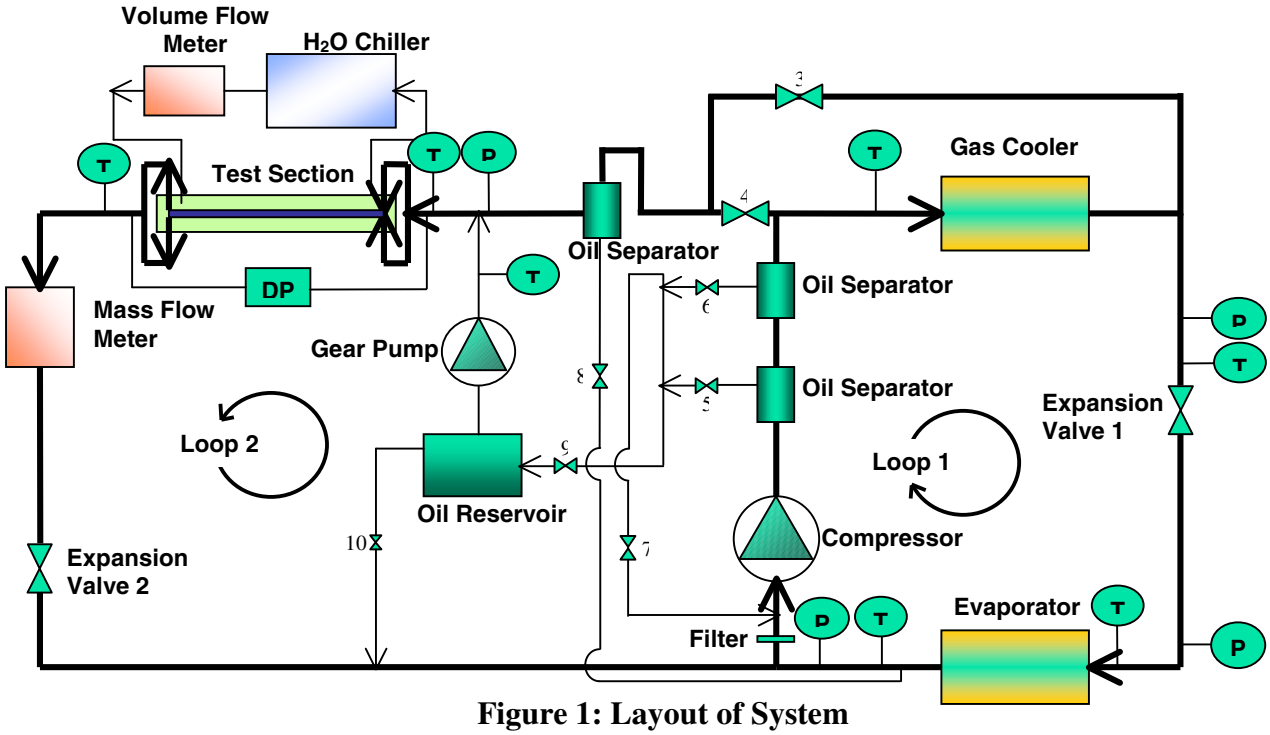

Figure 1: Layout of System

P, and T type thermocouples, labeled T, placed in-between each element of the VCS to make sure it is running effectively and allowing for the proper test conditions to be established.

The second loop of the experimental system branches from the first loop before and after the gas cooler. Each of these branches has a valve to regulate the amount of flow through them. This allows for the varying inlet temperature of the test section to be obtained by mixing the low temperature CO_2 (after gas cooler) with the high temperature CO_2 (before gas cooler). There is an accumulator and another oil separator placed before the test section at this point in an attempt to completely remove all oil from recirculating. The accumulator and oil separator drain connect back to the suction side of the VCS so that the oil in them is pulled out. As stated above, the two oil separators after the compressor drain to an oil reservoir. This oil reservoir is attached to a gear pump that can inject oil into the second loop before the test section, allowing for alteration of the OCR amount in the CO_2. In the secondary loop is the test section, which will be explained in detail later. A pressure transducer is placed before the test section and a differential pressure transducer is placed across the test section to obtain the outlet pressure. High accuracy Resistance Temperature Detectors (RTD's) are used before and after the test section to measure temperature. After the test section, the second loop has a mass flow meter and expansion valve 2. Expansion valve 2 controls the flow rate though the second loop, if it is closed then only the first loop will run and the whole system will act as a VCS. The heat transfer that occurs with the CO_2 and oil mixture is induced by H_2O flowing in the opposite direction over the micro channel inside of the test section. The H_2O is isolated in a third loop that consists of a

volume flow meter, two RTD sensors, a H_2O chiller to maintain its inlet temperature and an immersion heater to increase its inlet temperature.

The system tubing consists of stainless steel. Stainless steel nuts and ferrules were used at all connections. It was imperative to use stainless steel because of the high pressures that the system is expected to withstand. The majority of the tubing is 1/8" O.D., however 3/8" O.D. tubing is used from the evaporator outlet to the compressor suction, allowing for more efficient suction from the compressor. The whole system was built upon a steel frame rigging that lifts the system off the floor, preventing any parts from being in contact with leaking H_2O that may be coming from the H_2O chiller. This is especially important for all electrical components. The steel frame was built upon wheels that allowed it to be moved around the lab. This was essential in the beginning of the project when the lab was under construction and was in a state of constant disarray; however the system is now stationary.

A LabView program was developed to read all of the values of the system while it was running, such as temperatures, pressures and flow rates. LabView automatically created a MS Excel file so that the data was saved and could be analyzed at a later date. This will be described in more detail in the Instrumentation section.

The following procedures were developed for starting and running the system:

1. Close valves 1, 2, 3, 4, 9 and 10 as labeled in Figure 1. Completely open the valves between the oil separators and the suction line of the compressor: valves 5, 6, 7 and 8.
2. Turn on the compressor, thus pulling all of the oil in the system back to the compressor.

3. Let the compressor run for approximately 15 minutes. Make sure to watch the temperature on the PID controller attached to the discharge of the compressor, if this value exceeds 150°C then turn off the compressor. If the compressor must be shut off before the compressor runs for 15 minutes, let the compressor cool down and then run the compressor again, but make sure to keenly observe the temperature on the PID controller.
4. Once the compressor has run for approximately 15 minutes, turn the compressor off and leave the system idle for 30 minutes to an hour to cool down.
5. Completely close valves 7 and 8, then open them three full revolutions. This ensures there is pull from the suction line so that oil does not accumulate in the oil separators.
6. Open valves 1, 3 and 4 half way. These will have to be adjusted later to alter the inlet pressure and temperature to the test section to specified test conditions after the system has settled down, however at this point that is not important.
7. Leave valves 5 and 6 completely open.
8. Open valve 2 slightly, approximately 1 ½ turns. This adjusts the flow rate of the CO_2 through the test section. This setting will have to be altered once the system has reached steady state to adjust the mass flux to the specified test conditions.
9. Keep valves 9 and 10 closed. These will be adjusted later when it is needed to fill the oil reservoir with oil that will be injected into the CO_2 flow before the test section to vary the OCR amount.
10. The National Instruments LabView file, co2hpmain.vi, should be opened now if it is already not. The scan rate should be set to 5 seconds. Once the system has settled this can be increased, but in order to know what is happening until then a frequent scan rate is recommended. The graph selector should be on 'Refrig. Pressure' and the numeric selector should be on 'Refrig. Temp.'. The graph selector can be changed to 'Refrig. Temp.' to see the trend of the system over time as well. Finally, increase the test length to the desired amount and then press the 'Write On/Off' button to start saving the data to an MS Excel file.
11. Turn on the fans for the evaporator and the gas cooler.
12. Turn on the H_2O chiller. Adjust the temperature to its highest setting, 36°C, which it should already be set on.
13. Then, turn on the compressor via the switch on the circuit breaker mounted on the wall.
14. Watch the graphs on the National Instrument LabView to make sure the system is reacting as expected. It should take at least two hours for the system to reach any sort of steady state. (This can be limited if the pressure exceeds the testing condition wanted and the high side pressure is dropped by opening the main expansion valve, valve 1. However, the converse will not happen if the high side pressure is increased from its current level. An increase in the pressure by closing valve 1 slightly will take some time to re settle.)
15. Once the system has operated about 30 minutes without minor changes, it is ready to be adjusted to a test condition. Table 4 explains the valves to control for each test condition.
16. Each test should be run for one hour when the system is settled around the test conditions. Then the system should be adjusted to another test condition for testing.

Table 4: Changes to System to Adjust to Test Conditions

Test Condition	Alteration	Action
Inlet Temperature [°C]	Increase	Close valve 3 and/or Open valve 4
	Decrease	Open valve 4 and/or Close valve 3
Inlet Pressure [MPa]	Increase	Close valve 1
	Decrease	Open valve 1
Mass Flux [kg/m^{2}s]	Increase	Open valve 2
	Decrease	Close valve 2
Heat Flux [kW/m^2]	Increase	Decrease H_2O inlet temperature
	Decrease	Increase H_2O inlet temperature

The above describes the day to day procedures when running the system. There are also maintenance procedures that should be completed on a more periodic basis. The H_2O reservoir in the H_2O chiller should be emptied once a month. There is a screw plug in the back labeled, Reservoir Drain, that can be opened to allow the H_2O to empty. The H_2O should be collected and disposed so it does not spill on the floor. Then, the reservoir should be refilled with distilled H_2O, which can be found on the 2nd Floor of the Chemistry Building. Inhibitor must be added to the H_2O to prevent corrosion, hence the purpose of this task. Ten to fifteen ml's of inhibitor should be mixed with the distilled H_2O in the reservoir. The specifics on the inhibitor will be discussed in detail in the Lessons Learned section. The reservoir can be accessed by prying open the top of the H_2O Chiller and then unscrewing the cover, as shown in Figure 2.

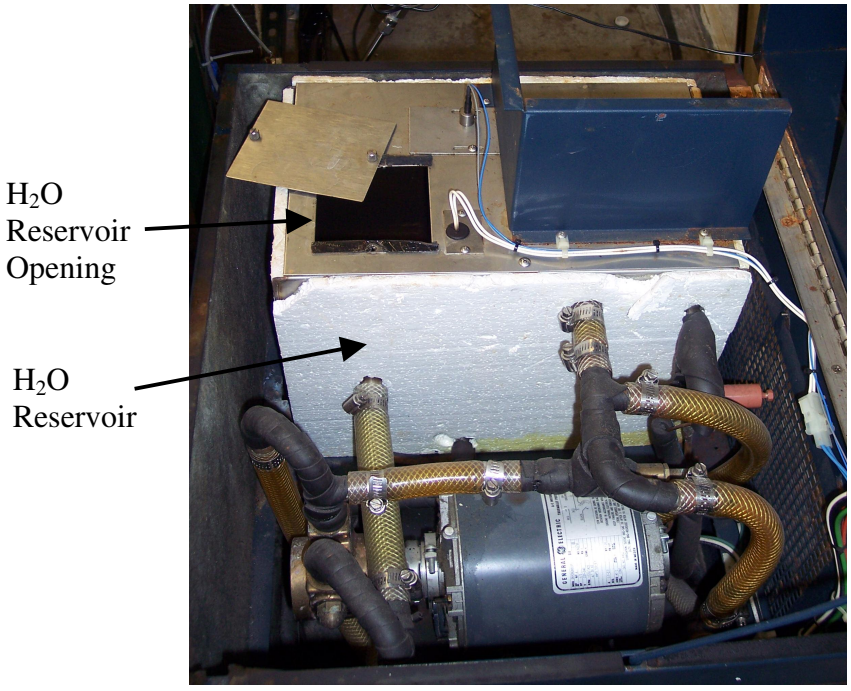

Figure 2: H_2O Chiller with Top Open

Under regular operation, oil starts to accumulate in the flow meter chamber since it is located at a low point in the system, causing skewed flow rate and density measurements. Therefore, the CO_2 flow meter must be cleaned about every two weeks. This is done by discharging the CO_2 from the system, disconnecting the flow meter fittings and then blowing compressed air through it for approximately 5 minutes Under normal operating conditions, the accuracy in the measurements of the mass flow meter can be up to ± 10%, which will be discussed in the Uncertainty section, so it is imperative to take all actions possible to limit any additional errors in their readings. The last precautionary measure to take is keeping the bearings of both the evaporator and gas cooler fans lubricated. Both fans are several years old and should be sprayed with WD-40 on their rotating parts at least once a month.

3.2 Test Section Detail

The test section in loop 2 of Figure 1 consists of a 600 mm micro channel with ten parallel circular ports that have a diameter of 1 mm each. A schematic of the micro channel can be seen in Figure 3. This micro channel was dip brazed by Ridge Engineering, Inc. to Aluminum 6061 headers that each has an outer diameter of 3/8". A picture of the micro channel brazed to the header can be seen in Figure 4.

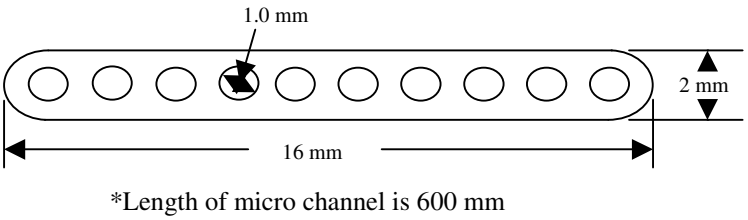

*Length of micro channel is 600 mm

Figure 3: Dimensions of Micro channel

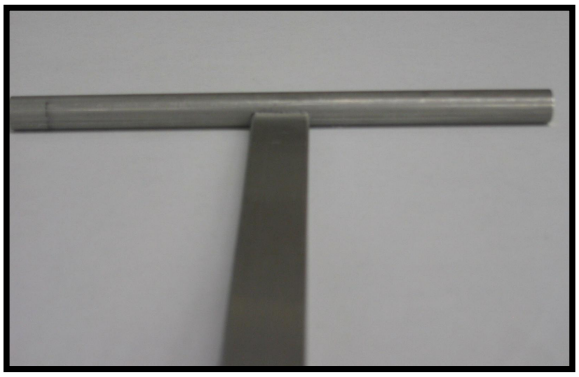

Figure 4: Aluminum 6061 Header Brazed to Micro channel

This assembly is encased in-between two clear polycarbonate sheets, which have had been milled on their mating sides. A portion of the sheets was cut out to allow placement of the micro channel to fit in-between the two polycarbonate sheets when they were assembled. Extra room was milled so that the H_2O could flow over the micro channel, allowing for the heat transfer to take place. Then vertical holes were cut in the sheets for bolts to lock the two surfaces together. Horizontal holes were drilled into the two sheets to make a groove for the Al headers to lie within. Figure 5 is a Pro-E drawing of the polycarbonate sheets and the machining that was performed on them. Once each was machined, they were fastened together by 4 20 bolts with the micro channel placed between them.

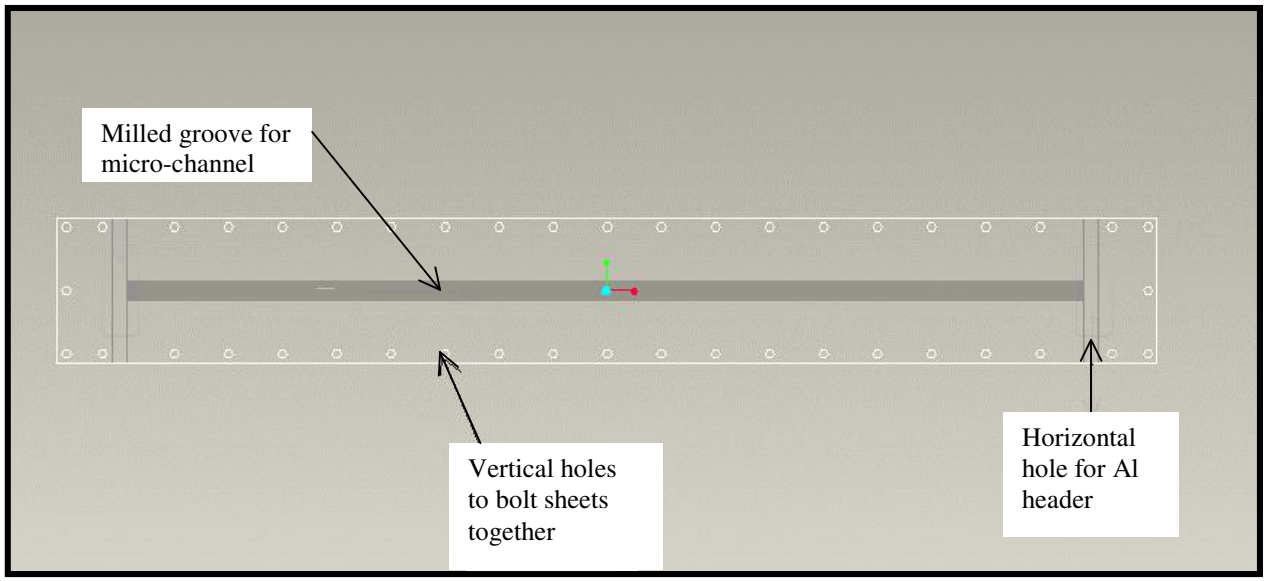

Figure 5: Polycarbonate Sheet Machined for Test Section

Figure 6 shows an assembled test section with the polycarbonate sheets tightened around a brazed micro channel. Although not shown here, the test sections used have a layer of epoxy placed in-between the mating sections of the sheets to eliminate any leaking of H_2O. Shown in Figure 6 is an NPT fitting placed right above the micro channel. Two NPT fittings provide access for the H_2O to enter and exit the milled out section of the polycarbonate sheets around the micro-channel. The inlet and the outlet NPT fittings for the H_2O are placed on opposite ends of the sheets. One is on the top while the other is on the bottom ensuring that the H_2O flows over the whole micro channel, horizontally and vertically.

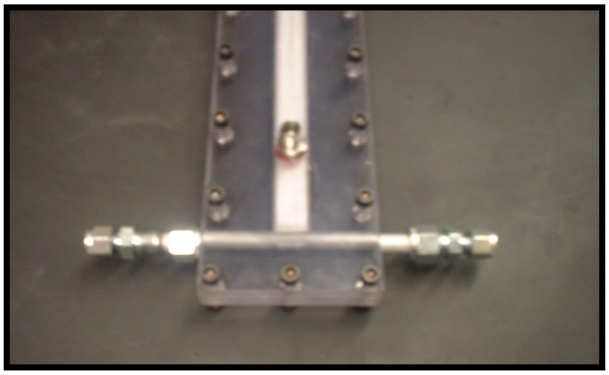

Figure 6: Test Section Assembled

A preliminary calculation was used in order to size the chamber where the H_2O would be flowing over the micro channel. The Gnielinski Correlation shown in Equation 1 was used to calculate a Nusselt number for the CO_2 side. The values for the Prandtl and Reynolds number were obtained by using the test conditions stated in Table 2.

$$Nu_{CO_2} = \left(\frac{f_{CO_2}}{8}\right) * \left(\frac{\left(\mathrm{Re}_{CO_2} - 1000\right) * \mathrm{Pr}_{CO_2}}{1 + 12.7 * \left(\frac{f_{CO_2}}{8}\right)^{1/2} * \left(\mathrm{Pr}_{CO_2}{}^{2/3} - 1\right)}\right) \quad \textbf{[1]}$$

Once this was calculated, the heat transfer coefficient for CO_2 was obtained from Equation 2.

$$h_{CO_2} = \frac{k_{CO_2} * Nu_{CO_2}}{D} \quad \textbf{[2]}$$

In order to obtain a heat transfer coefficient for H_2O, Equation 3 was used for laminar flow in annular tubes to determine a Nusselt number for H_2O. In this case, the tubes were rectangular sections so a hydraulic diameter was used. From D_{hi}/D_{ho}, where D_{hi} and D_{ho} can be seen from Figure 7, values can be obtained from heat transfer tables for Nu_{ii} and θ_i. (Munson)

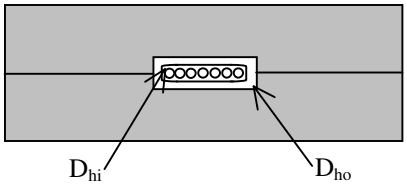

Figure 7: Hydraulic Diameters Used in Test Section Calculations

$$Nu_{H_2O} = \frac{Nu_{ii}}{\left(1 - \frac{Q_o}{Q_i}\right) * \theta_i} \quad \textbf{[3]}$$

The heat transfer coefficient for H_2O was calculated using Equation 2, making appropriate substitutions for H_2O instead of CO_2. Equation 4 was used to find the heat transfer between the fluids so that an optimum spacing between the micro channel and the outside

wall of the chamber could be found so that the H_2O had a temperature change greater than 2°C. Anything less than 2°C could amplify the error caused by inaccuracies in the temperature measurements.

$$\left[\dot{m} * \left(h_{in} - h_{out}\right)\right]_{CO_2} = \left[\dot{m} * C_p * \left(T_{out} - T_{in}\right)\right]_{H_2O} \quad \textbf{[4]}$$

3.3 Instrumentation

3.3.1 Compressor

The compressor being used is a CO_2 300 Series two-stage compressor by Dorin. It requires a 208 Volt, three phase power source and consumes 3 kW of power. This Dorin compressor can be observed in Appendix A. A PID controller was implemented with the compressor to make sure that it did not exceed a preset temperature and burn out the compressor. The PID controller was used to turn off the 208 Volt power supply if the outlet temperature of the compressor exceeded 160°C.

3.3.2 Heat Exchangers

The heat exchangers used for this project were from the CEEE lab. They both utilize micro channels to produce heat transfer with air flowing over them. The gas cooler is shown in Figure 8 and the evaporator in Figure 9.

Figure 8: Gas Cooler

Figure 9: Evaporator

3.3.3 Oil Separators

The oil separators used for this project are prototype CO_2 oil separators from Parker. Three are implemented and they each have a capacity to collect around 325 cm^3 of oil and are pictured in Appendix B.

3.3.4 Resistance Temperature Detectors

Since the change in temperature over the test section can be very small at certain test conditions, it was imperative to get accurate temperature devices to limit the error. Any slight change in the temperature readings could induce large errors in the results. Since most common T Type thermocouples have an error of ± 0.5°C, it was decided that they were not to be used. Instead, RTD's were purchased from Sensing Devices, Inc. that produces an error of ± 0.012°C. These RTD's are shown in Appendix C.

3.3.5 Pressure Transducers

Four Setra in-stream pressure transducers, Model # 280E, are used throughout the system and can be viewed in Appendix D. Three are utilized between components of the VCS to

ensure the cycle is working properly, while the last is placed directly before the test section. They can withstand pressure up to 20.68 MPa, well above the highest specified test condition. The uncertainty in pressure readings stated by Setra is 0.1%.

3.3.6 Differential Pressure Transducer

A differential pressure transducer is used over the test section to determine the outlet pressure of the CO_2. This device measures the pressure difference between two points and is used in this instance to reduce any errors that might occur from slightly offsetting calibrations in attempting to obtain a difference between two in-stream pressure transducers. The differential pressure transducer is made by GP:50 and is Model 215-C-PZ/HM, which can be seen in Appendix E. This model can withstand up to 68.94 MPa and reads a difference in pressure between 0 and 689.5 kPa. GP:50 claims the uncertainty in the values are 2.0%.

3.3.7 Mass Flow Meter

As illustrated in Figure 1, a mass flow meter is placed in the second loop of the system to measure the flow of CO_2 through the test section. A Micro Motion, Inc. coriolis mass flow meter was purchased for this task, specifically Model R025P. It covers a range of 0-30 g/s and can read both gases and liquids. It can also read slurries, mixtures of gases and liquids, with varying degrees of accuracy. In addition to measuring flow, the mass flow meter also measures the density of the fluid. This will become extremely valuable to the project when determining the OCR wt.% of the fluid. As the flow rate of the CO_2 decreases the error of the mass flow meter increases. At a flow rate that is 6 g/s, 20% nominal flow rate of 30 g/s, the error of the mass flow meter could be as large as 10%. The uncertainty in its density

measurements were quoted by Micro Motion as ±10 kg/cm^3. This model can be observed in Appendix F.

3.3.8 Volume Flow Meter

A volume flow meter is used to measure the flow of the H_2O passing thru the test section. This device was made by Sponsler Co, Inc. and is a turbine flow meter that has a range of 0-40 g/s. This flow meter is different from the Micro Motion unit in that it measures volume passing through its turbine. The density of the H_2O is measured by obtaining the temperature of the H_2O entering the test section from the inlet RTD. The mass flow rate of H_2O is calculated by multiplying the volume flow rate by the density of the H_2O. Sponsler Co. states a low repeatability of 0.25% in this model. This flow meter is shown in Appendix G.

3.3.9 H_2O Chiller

A H_2O chiller is used to maintain the temperature of the H_2O as it re-circulates over the test section. A NesLab HX-75 H_2O chiller, pictured in Appendix I, was inserted into the system. It holds approximately 15 liters of H_2O in its reservoir that it recirculates and cools by means of tap H_2O for heat transfer. The temperature range of the H_2O chiller is between 0 and ~36°C and the chiller can output H_2O at a rate up to 40 g/s.

3.3.10 Immersion Heater

Since the H_2O Chiller can only heat up the H_2O to a temperature of ~36°C, an alternative heating device was needed to meet the low heat fluxes specified in the test conditions. Accordingly, a screw plug immersion heater with a 500 Watt stainlesss teel heating element was purchased. Several copper fittings were soldered together to complete the

tubing over the element with an inlet and outlet for the H_2O. It is placed after the H_2O chiller and before the turbine flow meter in the H_2O loop. The heater is controlled by a variable autotransformer made by Staco Energy Products, Co. This allows the heater to be adjusted between 0 and 500 Watts so that the inlet H_2O temperature is exactly as needed. This heater must be grounded, in this case it is grounded to a circuit breaker, to prevent current from being induced in the H_2O and drastically altering the heat transfer balance. The immersion heater fully assembled and placed into the system can be seen in Appendix J.

3.3.11 Data Acquisition

In order to read the data, FieldPoint modules from National Instruments were used. One analog module, FP-AI-110 reads all of the pressure transducers and flow meters. A RTD module, FP-RTD- 122, was used for the four RTD's allowing for high accuracy temperature measurement. A thermocouple module, FP-TC-120, was used to convert all of the T type thermocouple millivolt outputs into degrees Celsius. All of these modules can be seen in Appendix H. These modules send their data to a LabView program which converts all of the raw data into pressures, flow rates and temperatures. An interface in LabView shows the current values and graphs showing the history of the system. LabView also stores all of the data in an MS Excel file with the time being saved in the farthest left column. A macro MS Excel file was created that implements a software program called XProps, which was created in-house by CEEE. This program calculates fluid properties, for example the density of the H_2O, the viscosity of both H_2O and CO_2 and the enthalpies of the CO_2 at different points, specifically before and after the test

section. From this information all calculations needed for this project can be performed in order to obtain the heat transfer coefficients and the pressure drop.

3.4 Completion of System

The system was assembled within one of the CEEE laboratories. A top and side view of the system can be seen in Figure 10 and Figure 11. Figure 10 shows the Micro Motion mass flow meter that is mounted with thetransmitter facing down . This is the prescribed way to install for gas flow and is the secondary method for liquids. Figure 1 shows a fan blowing on the compressor, to keep it from overheating since it easily reaches temperatures above 130°C. On the other side of the compressor is a PID controller that turns the compressor off if its discharge temperature exceeds 160°C. This is a precautionary measure to protect the compressor from overheating. Figure 12 shows the test section in the system covered with insulation held in place by duct tape. Both the inlet pressure transducer (left) and the differential pressure transducer (right) can be observed. It should be noted that valves were placed on both sides of the

Figure 10: Side View of Completed System

differential pressure transducer to protect it when charging the system and to allow for its removal without affecting the charged system, if necessary.

Figure 11: Top View of Completed System

Figure 12: Test Section in System

3.5 Lessons Learned

Several problems arose in early system testing. First, the system leaked rapidly. Since the system has to withstand up to 12 MPa, it was imperative that the system was leak tight to obtain accurate data and to maintain safety. Although leak prevention took a lengthy amount of time, this problem was eventually solved by the use of halogen leak detectors and by placing soapy water on the fittings. The use of the soap provided a visual method to observe if bubbles formed on the fittings due to a leak. Finally, it took time to understand that the system takes over twenty-four hours to stabilize on a pressure. Before knowing this it was thought that the system was leaking while in reality it was still just

settling. After all major leaks were corrected, the system was left untouched for at least a day and the pressures were correlated to the room temperatures. Since the system is not in a temperature controlled room, the pressure would increase and decrease in exactly the same proportion as the room temperature, in accordance with the ideal gas law.

After a month of preliminary testing, the one stage Dorin compressor initially implemented in the system broke down. When the system was taken apart it became apparent that there was a leak in the test section micro channel. Due to corrosion buildup on the micro channel a pinhole leak sprung, allowing for H_2O to enter the system. It is believed H_2O entered the compressor and caused it to reach temperatures exceeding 160°C, melting the electrical connections and causing permanent damage. To avoid harming another compressor and ruining another test section, distilled H_2O was used that had an inhibitor mixed in it. Further research into the problem showed that other research setups such as Neksa et al. (2001) used de-ionized H_2O, however there was no supply of de-ionized H_2O available. Working in the same manner as the de-ionized H_2O the inhibitor, a Potassium Silicate solution called Kasil 1 from the PQ Corporation, coats the metal surface preventing corrosive materials from attaching to the micro channel. Figure 13 shows the micro channel that was used for a month before the inhibitor was placed in the H_2O that sprung a leak damaging the one stage Dorin compressor. Figure 14 shows a micro channel that was used for a month with distilled H_2O and the inhibitor after the two stage Dorin compressor mentioned in the Instrumentation section was installed into the system. It is clear to see the corrosion buildup when the inhibitor was not implemented.

Figure 13: Micro Channel Used Without Inhibitor

Figure 14: Micro Channel Used With Inhibitor

As an additional safety measure, a PID controller was installed. A T Type thermocouple measures the compressor discharge temperature and turns off the voltage to the compressor if the temperature exceeds 160°C, thus disabling the compressor.

At this point the system was complete and baseline tests were initiated. It was immediately clear that the heat transfer balance between the CO_2 and H_2O side did not match. The calculations to determine the heat transfer can be seen in Equations 5 and 6.

$$Q_{CO_2} = \left[m * \left(h_{OUT} - h_{IN}\right)\right]_{CO_2} \quad \textbf{[5]}$$

$$Q_{H_2O} = \left[m * C_P * \left(T_{OUT} - T_{IN}\right)\right]_{H_2O} \quad \textbf{[6]}$$

Various test conditions were conducted, however the error level remained at 30% or larger. Figure 15 shows one of the original heat balance calculations for the system when the inlet conditions to the test section were as follows, P_{CO2} = 8.5 MPa and T_{CO2} = 120°C. As one

can see, the error produced after the system stabilized maintained a value above 50%, not an acceptable result.

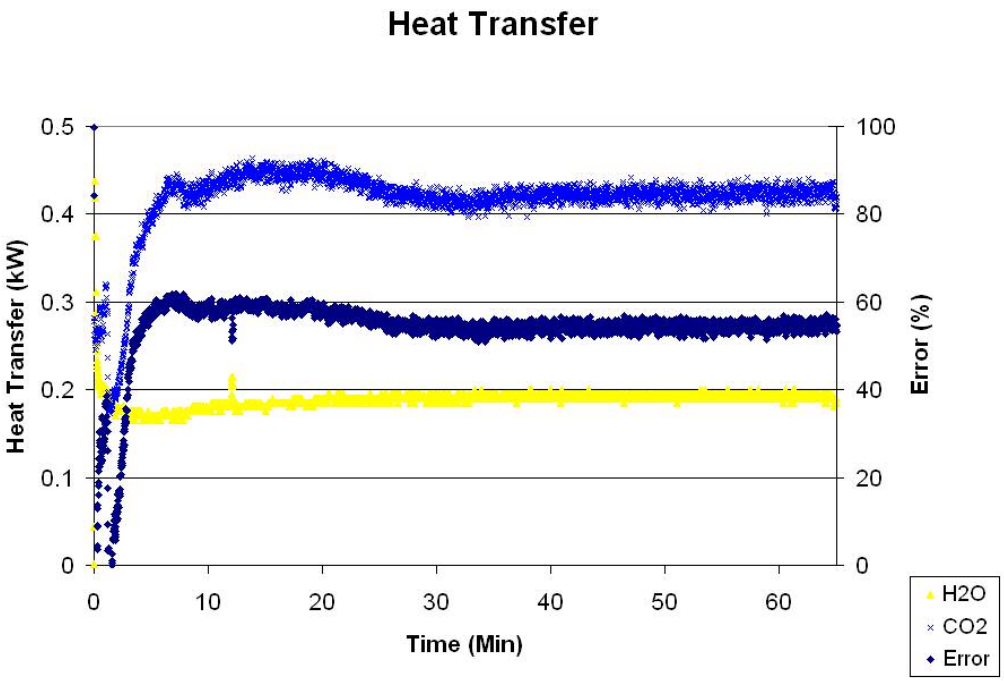

Figure 15: Heat Transfer Balance Before Alterations Were Made

In order to alleviate the error in the heat transfer balance the following steps were taken:

- The CO_2 mass and H_2O volume flow meters were re-calibrated.
- All four pressure transducers were re-calibrated.
- Temperature sensors were completed submerged into the flow (Before only the tips of the sensor were submerged, thus the length of the sensor in contact with flowing CO_2 and H_2O increased from ¼" to 3").
- Filters were added before the temperature sensors on the H_2O side to mix the flow, evenly distributing it.
- It was found that the original differential pressure transducer was not giving accurate values, thus it was replaced with the GP:50 model mentioned in the Instrumentation section.
- Temperature and pressure instrumentation were moved as close to the test section as possible, limiting the temperature lost through the stainless steel tubes and eliminating the pressure drops encountered do to bends in the tubing.
- Two additional RTD sensors were purchased so that both the CO_2 and H_2O temperatures were as accurate as possible (Before the H_2O side was being measured with T Type thermocouples, which have an accuracy of ± 0.5°C compared the RTD's that have an accuracy of ± 0.012°C).

- Oil was found recirculating in the test section loop, thus an accumulator and an oil separator were inserted before the test section. This appears to be the biggest and most frequently occurring problem faced.
- An appropriate range for testing the H_2O side was implemented.

Up to this point the accuracy of the heat transfers for the CO_2 and H_2O side were found by comparing the two. It was then decided to check the accuracy of the H_2O side alone by conducting a heat balance with a heating tape. A heating tape of 600 Watts was wrapped around the pipe and was insulated. The amount of heat produced by the heating tape was measured by a watt meter and was measured through the National Instruments analog module. Figure 16 shows the results recovered for this procedure, the pink represents the constant heat supplied by the heating tape, the purple represents the measured heat transfer of the water by Equation 6, and the gray is the percent error between the two.

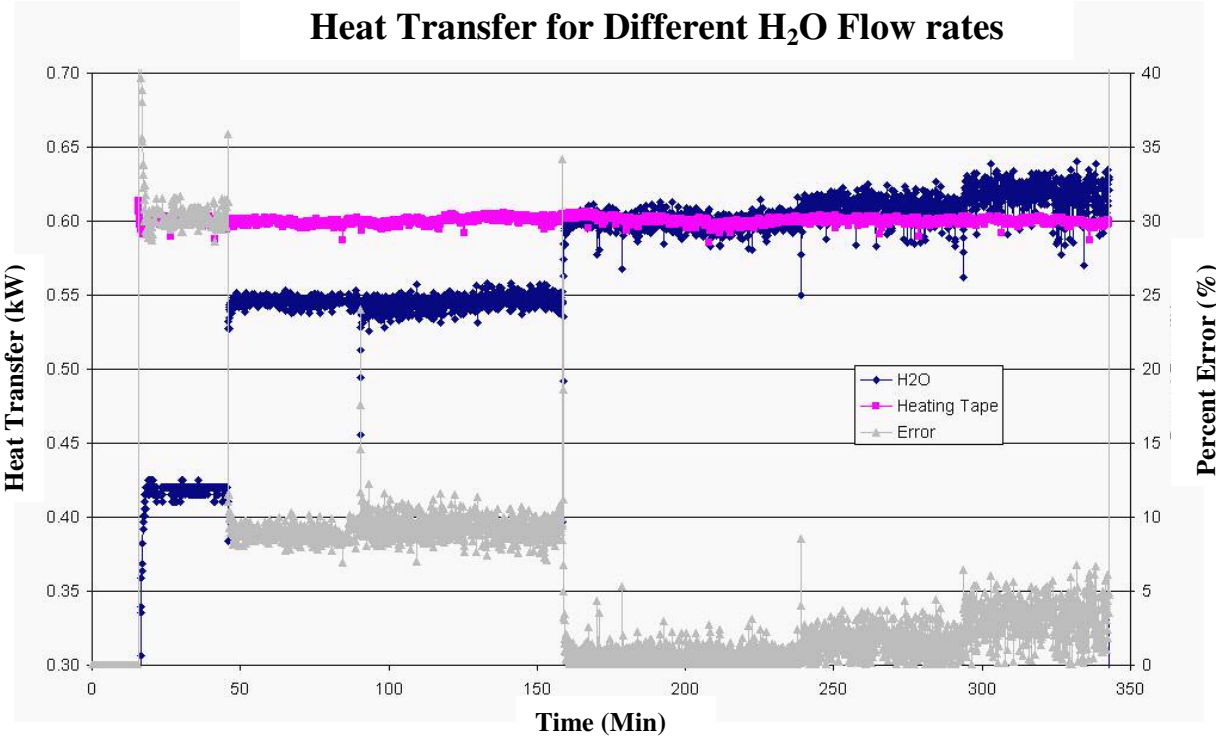

Figure 16: Heat Transfer between H_2O and Heating

The changes seen in the H_2O measured heat transfer were due to adjustments made to the H_2O's flow rate. Initially, the H_2O's flow rate was 40 g/s, however this was lowered at the 45^{th}, 80^{th}, 160^{th}, 240^{th}, and the 295^{th} minutes. The Sponsler Co. turbine flow meter is an accurate device; however errors do occur when the flow through it is less than 5 g/s. It is believed the larger error observed in the first three flow rates were due to the temperature readings. With larger flow rates the ΔT is smaller and at the time of this procedure T Type thermocouples were still being implemented. Since these thermocouples have an error of ± 0.5°C each there is the possibility that when the thermocouples are used to calculate differences they could produce errors up to ± 1.0°C. For the first three tests the ΔT's were in the range of 3.5 to 7°C, if the T Type thermocouples were slightly off they could cause the large deviations seen. The fourth test produced the best results with the heating tape and allows for the operator of the system to aim for this specific range of an H_2O flow rate around 10 g/s and a temperature difference greater than 10°C. If this range is employed during testing with the cross flowing CO_2, it can be assumed the results from the H_2O side are justifiable. The fifth and sixth tests produced slightly larger errors because the flow rates of the H_2O side were around or less than 5 g/s, the range were the accuracy of the turbine flow meter worsens.

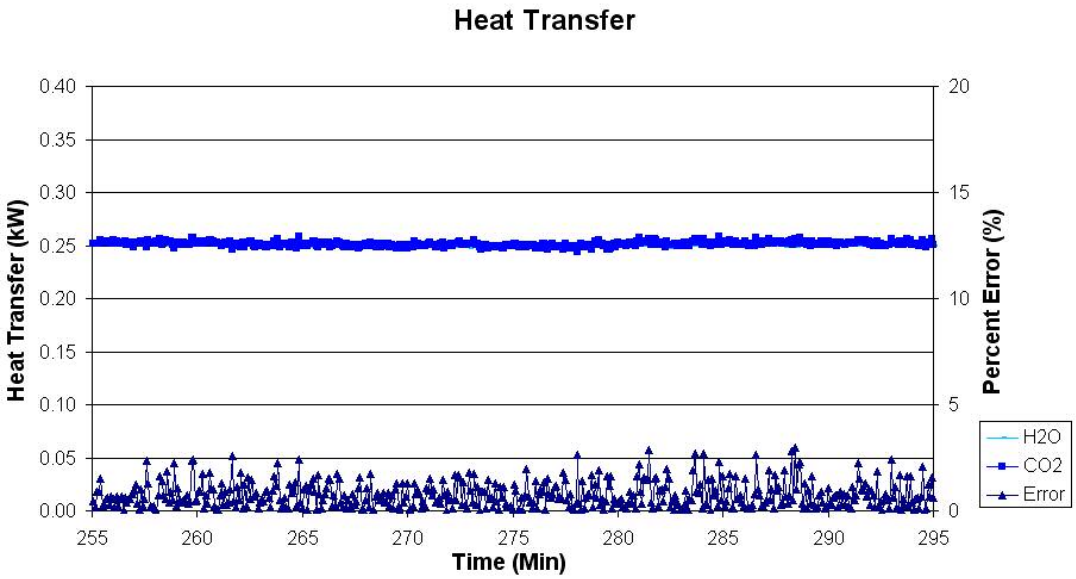

Figure 17: Improved Heat Transfer Balance of System

After all of the stated alterations were made, the error was reduced to around ± 8%. Figure 17 shows the heat transfer results and the corresponding error for data taken at the end of my time on the project. The average error for this test was 0.75%, showing a vast improvement from the average error at the outset of the project.

4 Results

4.1 Uncertainty

Although the above steps resulted in a much improved heat transfer error, there is error that can never be completely eliminated. This is especially true in the tests taken around 8 MPa, which are conducted close to the critical point of CO_2, 31.1°C and 7.38 MPa. In this range of values a small deviation in the measured temperature or pressure can greatly alter the calculated enthalpy as can be seen in Figure 18. Since the inlet temperatures for the test conditions range from 70°C to 100°C, which is far away from $T_{CO2,Crit}$, this is not an issue in regards to temperature. This is also true for the inlet pressure conditions of 10 and 12 MPa, however the tests conducted at 8 MPa are susceptible to this unavoidable error since they are so close to $P_{CO2,Crit}$.

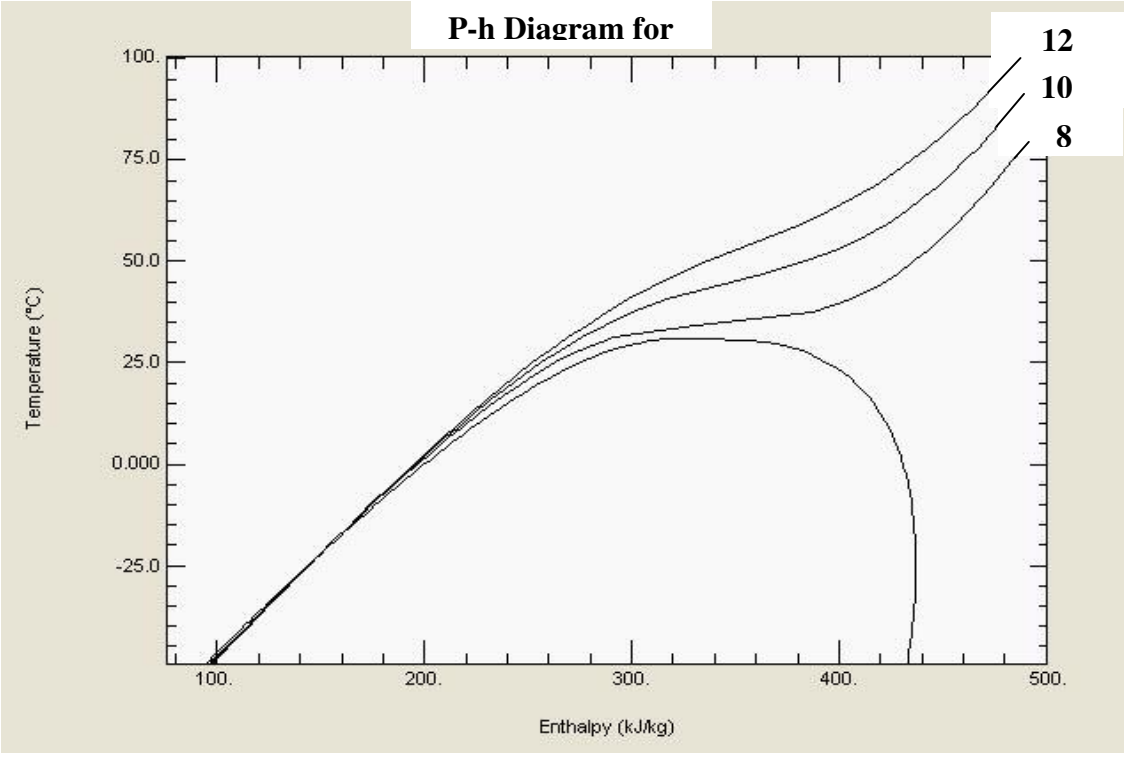

Figure 18: P-h Diagram for CO2 with Isobars

A second unavoidable error is that generated by the inaccuracies of the measuring devices: RTD's, flow meters and pressure transducers. The uncertainty of each is listed in Table 5.

Table 5: Accuracy Deviations of Measurement Apparatuses

Apparatus	Units	Absolute Uncertainty	Relative Uncertainty (%)
CO_2 Flow Meter (Micro Motion, Model R250P)	kg/s		0.1
CO_2 P_{inlet} (Setra, Model 280E)	kPa		0.001
CO_2 P_{diff} (GP:50, Model 215)	kPa		0.02
CO_2 T_{in} (Sensing Devices, RTD)	°C	0.012	
CO_2 T_{out} (Sensing Devices, RTD)	°C	0.012	
H_2O Flow Meter (Sponsler Co.Turbine)	kg/s		0.0025
H_2O T_{in} (T Type Thermocouple)	°C	0.012	
H_2O T_{out} (T Type Thermocouple)	°C	0.012	

The most significant error is that of the CO_2 flow meter. Due to budget constraints a high accuracy mass flow meter was not purchased, instead settling on the model stated in the Instrumentation section, R025P. For liquid flowing through the R-Series mass flow meter the deviation is ± 0.5 % and for gases the deviation is ± 0.75 %. Figure 19 shows the accuracy for the R-Series flow meter when a natural gas is flowing. The R025P model used in this system has a stated range of 0 – 50 lb/min. The figure clearly shows how the accuracy quickly diminishes as the flow rate decreases. The situation is magnified for this project because low mass flow rates are needed to obtain the specific mass fluxes stated in the test conditions. The distribution of these mass flow rates can be observed with their corresponding conversions in Table 6. Since the largest flow rate needed is 1.16 lb/min, one can observe from Figure 19 that the accuracy is not even shown. The technical

representatives for Micro Motion, Inc. gave the absolute uncertainty at approximately 10% and larger for smaller flow rates, leading to the greatest source of error in this project.

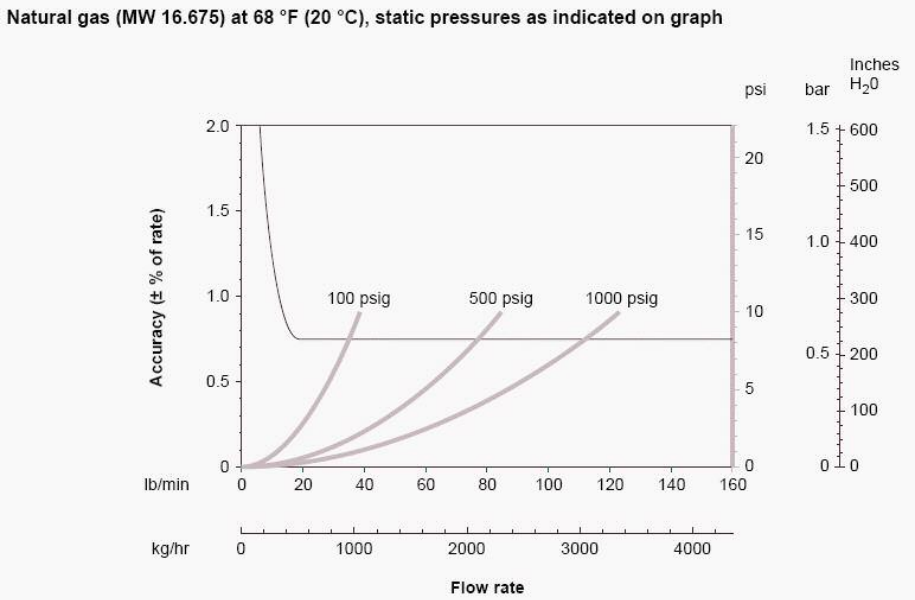

Figure 19: Accuracy of R025P Micro Motion Mass Flow Meter (Emerson)

Table 6: Flow Rates Corresponding to Mass Flux Test Conditions

Mass Flux [kg/m^{2}s]	CO_2 Flow rate [g/s]	CO_2 Flow rate [lb/min]
400	3.5	0.4629708
600	5.25	0.6944562
800	7	0.9259416
1000	8.76	1.15875

An error propagation analysis was performed using Engineering Equation Solver (EES) with the errors for the measuring apparatuses illustrated in Table 5. The analysis was performed with data taken for a test where the conditions were: $P_{in,CO2}$ = 8.04 MPa, $T_{in,CO2}$ = 69.87 °C, m_{CO2} = 400.1 kg/m^{2}s and Q_{CO2} = 15.56 kW/m^2. Table 7 shows the error propagation for the CO_2 heat transfer could be up to 10% and Table 8 shows the error propagation to be 0.3% for H_2O.

Table 7: Error Propagation of CO_2 Side

Q_{CO2} (W) 263.5 ± 26.37	
Apparatus	**Percent of Error (%)**
CO_2 Flow Meter (Micro Motion, Model R250P)	99.89
CO_2 P_{inlet} (Setra, Model 280E)	0.10
CO_2 P_{diff} (GP:50, Model 215)	0.00
CO_2 T_{in} (Sensing Devices, RTD)	0.00
CO_2 T_{out} (Sensing Devices, RTD)	0.01

The error when comparing the two calculated heat transfer amounts is 4.13%, which is equivalent to a difference of 10.9 W's, however, Table 7 shows that the possible error in the CO_2 side alone could be ± 26.37 W's. Therefore, the 4.13% error measured is acceptable since it is within the projected uncertainty calculated by EES. Confirming the above discussion about the large error possible by the CO_2 flow meter, as seen in Table 7 it accounts for 99.89% of the error calculated by EES. The only way to decrease this error would be to purchase a higher accuracy flow meter. As can be observed in Table 8, the Sponsler Co. turbine flow meter does not account for an error on the H_2O side because Sponsler states an accuracy of 0.25%.

Table 8: Error Propagation of H_2O Side

Q_{H2O} (W) 252.6 ± 0.7571	
Apparatus	**Percent of Error (%)**
H_2O Flow Meter (Sponsler Co.Turbine)	0.00
H_2O T_{in} (T Type Thermocouple)	49.49
H_2O T_{out} (T Type Thermocouple)	50.51

The final reason for uncertainty could be heat lost to the ambient surroundings. Even though the complete test section was covered with an inch and a quarter of insulation, there is still some heat exchange between the room at ambient temperature and the water temperature flowing through the test section. Calculations using EES were used to estimate a value of heat lost. The following three equations were found in the ASHRAE Handbook: Fundamentals, in relation to natural convection heat transfer coefficients. The first natural air heat transfer coefficient is for a vertical small plate in the laminar range, which refers to the H_2O flowing and can be expressed as Equation 7. The ΔT refers to the change in temperature of the H_2O side and L is the length that the H_2O flows in the test section.

$$h_1 = 0.29 * \left(\frac{\Delta T}{L} \right)^{0.25} \quad \textbf{[7]}$$

Equation 8 is for the natural air heat transfer coefficient for a small horizontal plate, facing upward when heated in the laminar range.

$$h_2 = 0.27 * \left(\frac{\Delta T}{L} \right)^{0.25} \quad \textbf{[8]}$$

Equation 9 is for the natural air heat transfer coefficient for a small horizontal plate, facing downward when heated.

$$h_3 = 0.12 * \left(\frac{\Delta T}{L} \right)^{0.25} \quad \textbf{[9]}$$

With the following information known, overall thermal resistances where calculated for all four sides of the test section, as diagramed in Figure 20. The sides that the above natural convection heat transfer coefficients apply are labeled as well as the two lengths of the polycarbonate test section, L_a and L_b. The length of the insulation, L_{ins}, is constant at

2.875 cm's on all four sides. Equation 10 and 11 are the thermal resistances for the two vertical sides and for the two horizontal sides. R_a refers to both vertical sides while R_b refers to both the top and bottom, or horizontal sides.

$$R_a = 2*\left(\frac{1}{A_a}\right)*\left[\left(\frac{1}{h_1}\right)+\left(\frac{L_{ins}}{k_{ins}}\right)+\left(\frac{L_a}{k_{poly}}\right)+\left(\frac{1}{h_{H_2O}}\right)\right] \quad \textbf{[10]}$$

$$R_b = \left(\frac{1}{A_b}\right)*\left[\left(\frac{1}{h_2}\right)+\left(\frac{1}{h_3}\right)+\left(\frac{2*L_{ins}}{k_{ins}}\right)+\left(\frac{2*L_b}{k_{poly}}\right)+\left(\frac{2}{h_{H_2O}}\right)\right] \quad \textbf{[11]}$$

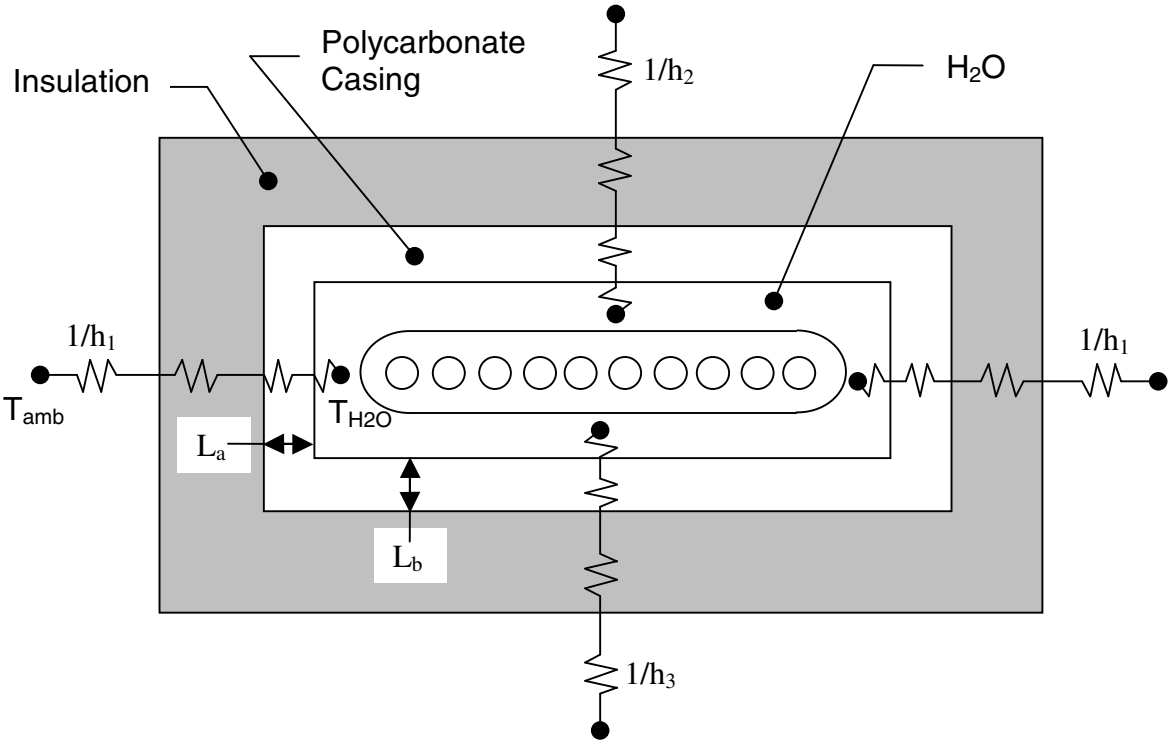

Figure 20: Thermal Resistances of Test Section for Heat Lost to Ambient

Finally, Equation 12 estimates the amount of heat lost to the room. Revisiting the same test used above in this section, the ambient temperature was around 30.5 °C and the average temperature of the H_2O was 35.2 °C. For this condition, EES calculated a heat loss of 1.24 W. This is extremely small and for this test was concluded as negligible.

However, this procedure still needs to be carried out for all tests, particularly those where the H_2O is heated to meet the lower heat flux conditions. It is imperative under such conditions because the ΔT between the flowing H_2O and the room temperature will be greater than in the test shown above where they only differ by ~4.7 °C. The larger the difference between $T_{H2O,Avg}$ and T_{Amb} than the greater Q_{Lost} will be, inducing a larger heat transfer balance error.

$$Q_{Lost} = \frac{T_{H_2O,AVG} - T_{AMB}}{R_a + R_b} \quad \textbf{[12]}$$

4.2 Wilson Plot

Before starting to run tests under the targeted conditions, the Wilson Plot method must be implemented. Between the complicated geometry of the test section and the low Reynolds number of the H_2O, there are no existing correlations to obtain the heat transfer coefficient for the H_2O side that are applicable. Common correlations for single phase liquids are for turbulent flow. Since the heat transfer coefficient for the H_2O side is an essential parameter in this project, a modified Wilson Plot method is the only way to avoid using unsuitable correlations that will not produce desired accuracy. The basis of the Wilson Plot is a data reduction procedure, which is used to find a Dittus-Boelter type correlation by plotting *U* vs. Re.

The equation for the overall heat transfer coefficient, *U*, can be seen in Equation 13. In this equation, A is the area of heat exchanged and R_w is the thermal resistance of the wall.

$$\frac{1}{U} = \frac{1}{h_{CO_2}} + \frac{1}{h_{H_2O}} * \frac{A_{H_2O}}{A_{CO_2}} + R_w \quad \textbf{[13]}$$

The Dittus-Boelter correlation for the H_2O heat transfer coefficient is given in Equation 14, where k is the thermal conductivity and D_h is the hydraulic diameter of the section that the H_2O flows through.

$$h_{H_2O} = C * \left(\mathrm{Re}^m \, \mathrm{Pr}^n \, \frac{k}{D_h} \right)_{H_2O} \quad \textbf{[14]}$$

Substituting Equation 14 into 13 creates Equation 15. Equation 15 can be written as Equation 16; Equations 17, 18, 19 and 20 show all the substitutions used. (Kuang et al.)

$$\frac{1}{U} = \frac{1}{C} * \left(\frac{1}{\mathrm{Re}^m \, \mathrm{Pr}^n \, k / D_h} \right)_{H_2O} + \left(\frac{1}{h_{CO_2}} * \frac{A_{H_2O}}{A_{CO_2}} + R_w \right) \quad \textbf{[15]}$$

$$Y_1 = A * X_1 + B \quad \textbf{[16]}$$

$$Y_1 = \frac{1}{U} \quad \textbf{[17]}$$

$$X_1 = \frac{1}{\mathrm{Re}^m \, \mathrm{Pr}^n \, k / D_h} \quad \textbf{[18]}$$

$$A = \frac{1}{C} \quad \textbf{[19]}$$

$$B = \frac{1}{h_{CO_2}} * \frac{A_{H_2O}}{A_{CO_2}} + R_w \quad \textbf{[20]}$$

Additionally, Equation 15 can be rewritten as Equation 21, which is then simplified to Equation 22. Again, Equations 23, 24, 25 and 26 show all of the substitutions introduced to obtain Equation 22 from Equation 21. (Kuang et al.)

$$\left(\frac{1}{U} - B \right) * \left(\mathrm{Pr}^n \, k / D_h \right)_{H_2O} = \frac{1}{C} * \left(\frac{1}{\mathrm{Re}^m} \right)_{H_2O} \quad \textbf{[21]}$$

$$Y_2 = D * X_2 + E \quad \textbf{[22]}$$

$$Y_2 = \ln\left\{\left(\frac{1}{U} - B\right) * \left(\mathrm{Pr}^n \, k / D_h\right)_{H_2O}\right\} \quad \textbf{[23]}$$

$$X_2 = \ln(\mathrm{Re}) \quad \textbf{[24]}$$

$$E = -\ln(C) \quad \textbf{[25]}$$

$$D = -m \quad \textbf{[26]}$$

The steps to complete the Wilson Plot method are as follows:

1. Set CO_2 flow rate, pressure, and inlet temperature while maintaining liquid status for both inlet and outlet
2. Conduct test series at various H_2O flow rates
3. Maintain constant heat transfer between both liquids
4. Calculate the overall heat transfer coefficient
5. Guess m, and perform curve fitting for Equation 16
6. Get B value from curve fitting
7. Perform curve fitting for Equation 22
8. Get D value from curve fitting
9. Check D = -m
10. If not, guess another value for m until -m and D become equal

In order to maintain the liquid phase of CO_2, the Wilson Plot will have to be run at test conditions below the critical point of CO_2. To accomplish this, a Suction Line Heat Exchanger (SLHX) was inserted into the system, as seen in Figure 21. Since the SLHX introduced heat transfer between the gas cooler outlet (30°C) and the evaporator outlet (17.5°C), the temperature of the CO_2 entering the test section was reduced from what would have normally been the gas cooler outlet temperature. With the pressure being maintained at 7 MPa, the temperature needed to be lower than CO_2's saturation

temperature at 7 MPa, which is 28.68°C. The average inlet temperatures of the CO_2 to the test section obtained by using the SLHX for the eight tests taken were 26.28°C. During the Wilson Plot, the refrigerant was maintained as a liquid by keeping its inlet temperature at $T_{CO2,in}$ = (26.28 ± 0.2)°C and the inlet pressure at $P_{CO2,in}$ = (7.0 ± 0.04) MPa. The heat flux was kept constant at Q = (4.65 ± .06) kW/m^2 and the mass flux was also held constant at m = (791 ± 4.9) kg/m^{2}s. All measurements were taken once the test system conditions reached a steady state and the National Instruments modules logged all of the data to the LabView file. Data were taken every 5 seconds for a duration of an hour and the calibration was made with a total of 8 different H_2O mass flow rates, m = (4.54 to 18.06) g/s.

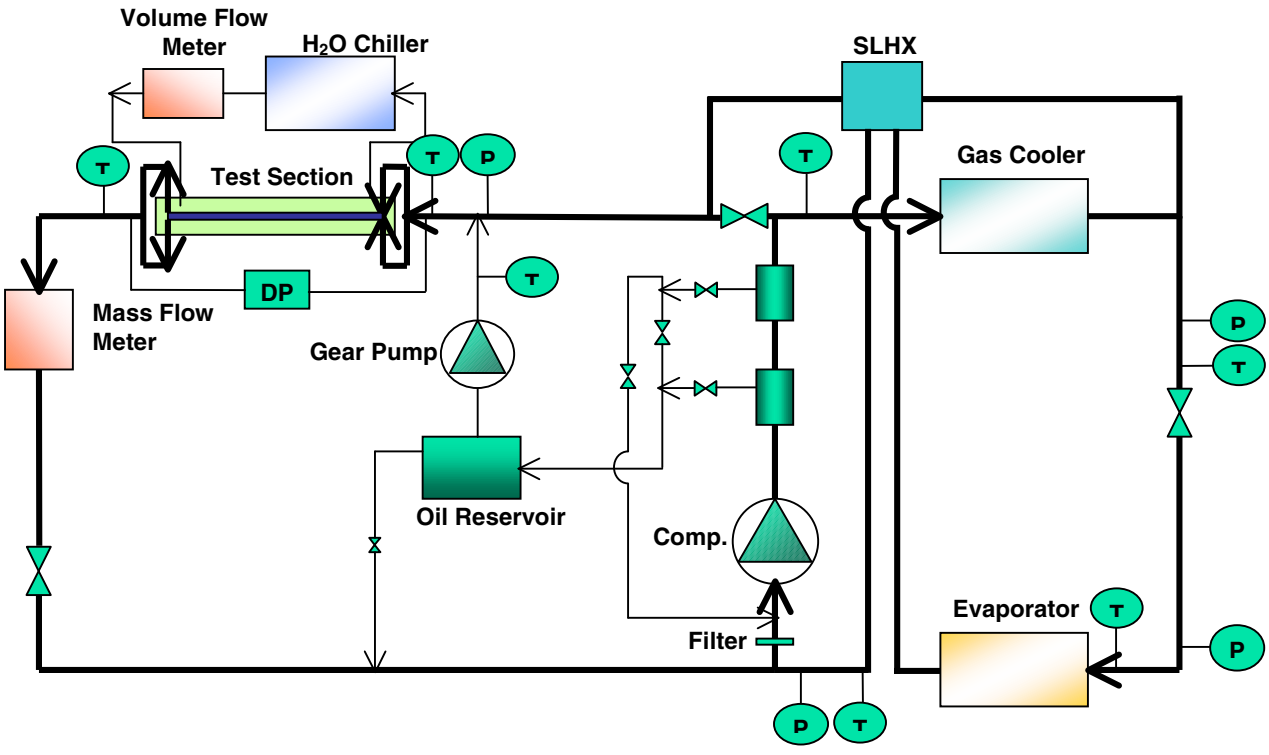

Figure 21: System with SLHX

An iteration process was incorporated to determine what m value corresponds to an equal but opposite D value (m = -D). In order to determine Y_1, it was needed to obtain U. This was done by using Equation 27 and solving for U. Both Q and LMTD were obtained from the measured data and A, which is the heat transfer area between the two fluids, is known from the geometry of the test section.

$$Q = U * A * LMTD \quad \textbf{[27]}$$

The process to calculate the LMTD is as follows:

- Subtract the H_2O outlet temperature from the CO_2 inlet temperature, which equals DT1
- Subtract the H_2O inlet temperature from the CO_2 outlet temperature, which equals DT2
- Divide DT1 by DT2. If 0.999 < DTR < 1.001, then go to (A), if not, proceed to (B)

$$\text{(A)} \quad LMTD = \frac{DT1 + DT2}{2}$$

$$\text{(B)} \quad LMTD = \frac{DT1 - DT2}{\ln(DTR)}$$

U is obtained by dividing Q by the heat transfer area and the calculated LMTD. From this information Y_1 is known. In order to calculate X_1, EES was used to calculate the thermal conductivity and the Prandtl number of H_2O from the measured data taken during the tests. A value of 0.4 was used for n because the H_2O is being heated, instead of a value of 1/3 which would be used if the H_2O was being cooled. The hydraulic diameter that is used to calculate both the Reynolds number and X_1 is obtained by using Equation 28.

$$D_h = \frac{4 * Cross\_Sectional\_Area}{Wetted\_Perimeter} \quad \textbf{[28]}$$

The cross-sectional area is found by subtracting the cross-sectional area of the micro channel from the cross-sectional area of the grooved out section between the two mating polycarbonate sheets. The wetted perimeter consists of both the outside perimeter of the grooved out section of polycarbonate plus the perimeter of the outside of the micro channel. All of the information is now known to graph X_1 vs. Y_1, which can be seen in Figure 22.

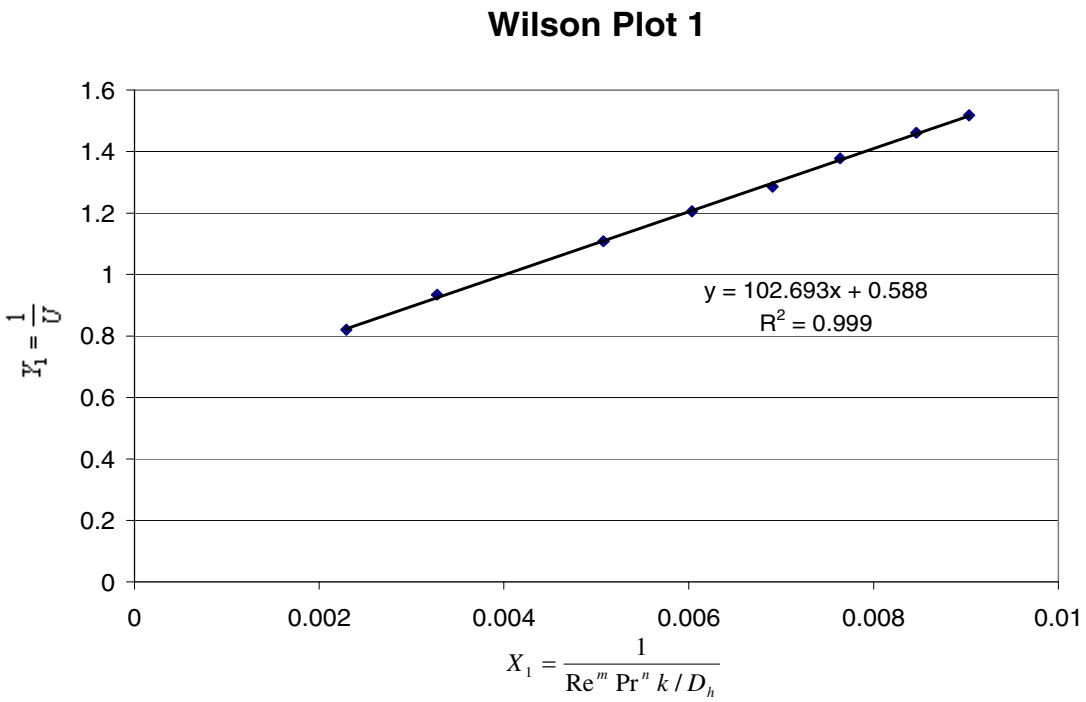

Figure 22: Wilson Plot for Water Heating

The next step in the Wilson Plot is to plot the logarithmic graph. As its name infers, X_2 is obtained by taking the natural log of the H_2O's Reynolds number. Y_2 is found by using much of the same information used for X_1, however it is re-arranged as can be seen in Equation 23. The B value seen in Equation 23 is the Y-intercept of the line of best fit shown in Figure 22, 0.588. The value of m, which is the power the H_2O Reynolds number is raised to, was iteratively changed to alter B. By varying B, the plotted data in Figure 23

changes causing the line of best fit for the logarithmic graph to be modified. When m is a value that causes the slope in Figure 23 to be equal but opposite (m = -D), then the Wilson Plot method has been achieved.

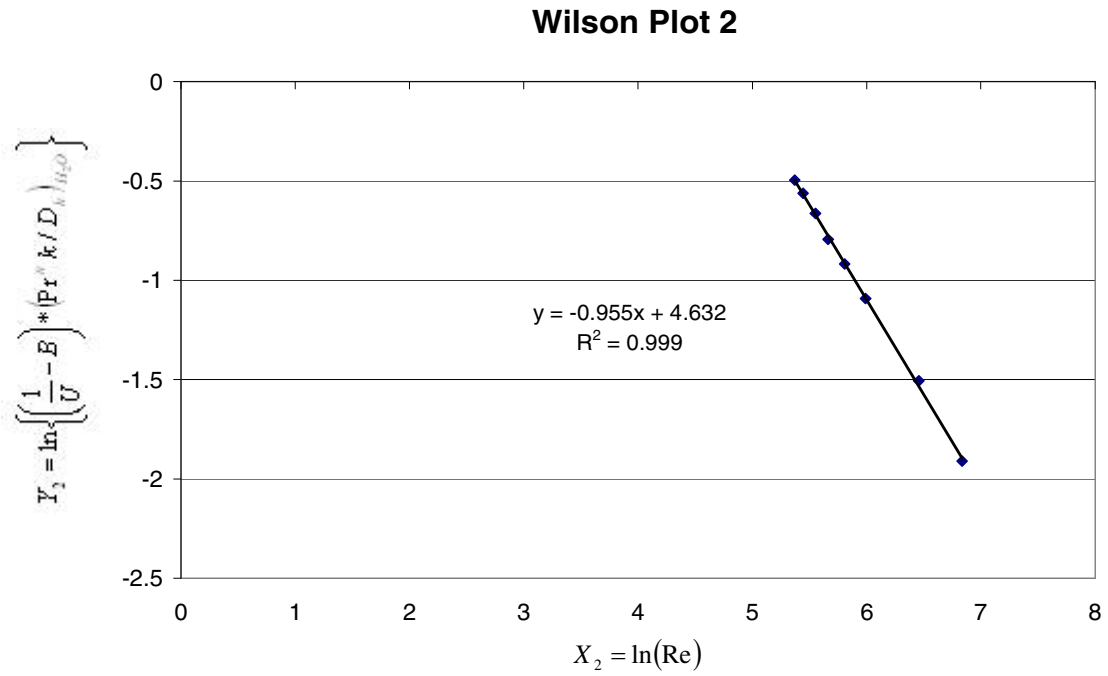

Figure 23: Logarithmic Wilson Plot for Water Heating

A line of best fit can be observed on both graphs as well as their R-squared values. Their R-squared values are close to 1.0 and the inserted m value equaled the negative slope in the logarithmic Wilson Plot graph, also known as D. This method was successfully completed. The plot gave the following values:

$$C = 0.009738 \quad \text{and} \quad m = 0.95478$$

From this information, the calibrated equation for the water side heat transfer coefficient (h_{H2O}) during heating mode is:

$$h_{H_2O,Heating} = 0.009738 * \mathrm{Re}^{0.95478} * \mathrm{Pr}^{0.4} * \lambda / d_{hyd} \quad \textbf{[29]}$$

From Equation 29, a heat transfer co-efficient can be calculated for each individual m_{H2O}. A graph showing these heat transfer coefficients is shown in Figure 24, it includes a line of best fit and its associated R-squared value.

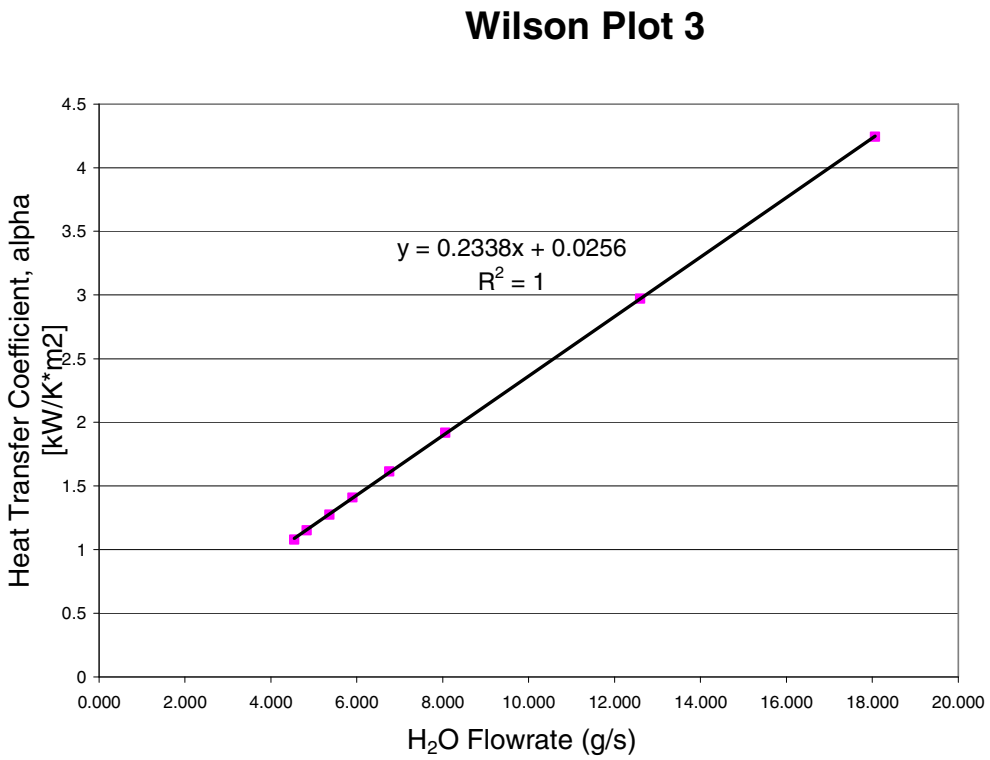

Figure 24: Calculated H_2O Heat Transfer Co-efficient for given H_2O Flow Rate

From this equation, a heat transfer co-efficient for H_2O can be easily calculated for each test run. Then, by use of Equation 30 the heat transfer co-efficient for CO_2 can also be determined for each test. R_w is the thermal resistance of the wall and is considered negligible; therefore it is omitted in the calculation. Both A_{H2O} and A_{CO2} are known and $UA_{Overall}$ is solved by knowing the heat transfer obtained during the test and then dividing

that by the calculated LMTD. Since an equation for h_{H2O} was just derived the only unknown is the heat transfer co-efficient for the CO_2, thus allowing for a simple solution after some algebraic manipulation.

$$\left(\frac{1}{UA}\right)_{Overall} = \left(\frac{1}{hA}\right)_{H_2O} + \left(\frac{1}{hA}\right)_{CO_2} + R_W \qquad \textbf{[30]}$$

4.3 Data

Unfortunately, the complete set of 864 tests for the conditions listed in Table 2 was not fulfilled. However, a limited amount of tests that are within the test condition range were completed and the important characteristics to these tests can be seen in Table 9.

Table 9: Test Conditions for Five Data Points Taken

Test	P_{inlet} [MPa]	T_{inlet} [°C]	Mass Flux [kg/m^{2}s]	Heat Flux [kW/m^2]	OCR [wt.%]	ΔP [kPa]	h_{CO2} [kW/m^{2}K]	Heat Transfer Error [%]
1	7.99	70.30	397.04	10.19	6.58	10.95	2.04	8.14
2	7.96	70.28	399.69	15.11	6.60	10.58	1.37	1.49
3	8.88	69.30	397.40	14.82	8.54	7.47	1.62	0.75
4	9.25	72.06	394.90	15.28	9.50	6.36	1.88	2.62
5	9.88	69.32	392.34	14.87	10.72	4.51	1.83	2.42

Every part of the tests went smoothly except that the OCR level that was circulating with the CO_2 was never controlled, even after the addition of the third oil separator and accumulator before the test section. No oil was injected into the flow, so the OCR level during these tests should have been 0 wt.%. The method used to compute the OCR was to compare the density the Micro Motion mass flow meter measured of the oil and the CO_2 mixture, ρ_{Mix}, versus a theoretical density for the mixture that was calculated in EES. Equation 31 was used to determine the theoretical density of the oil and this was used in

Equation 32 to determine a value for the OCR. Equation 31 was developed by the Idemitsu Company, from whom the PAG oil was purchased.

$$\rho_{Oil} = 1009.8 - 0.7 * T_{CO_2} \quad \textbf{[31]}$$

$$\rho_{Mix} = \frac{\rho_{Oil} * \rho_{CO_2}}{\left(\rho_{Oil} * (1 - OCR)\right) + \left(\rho_{CO_2} * OCR\right)} \quad \textbf{[32]}$$

Using this method, the OCR level was measured for all data points taken. The results were not favorable, since the OCR varied between 6.58% and 10.72%. Either there was still an abundance of oil circulating, or that the ±10 kg/cm^3 accuracy of the Micro Motion density measurements were not as accurate as needed. Both of these situations are discussed with plausible solutions in the Future Work section of this paper.

4.4 Comparison to Correlations

4.4.1 Heat Transfer

From the data received and the Wilson Plot mentioned above, calculating the heat transfer coefficient for CO_2 was completed by several simple steps. The heat transfer coefficient for H_2O was computed by using the equation obtained from the Wilson Plot method. Next, Equation 33 is calculated. The same method for solving the LMTD mentioned earlier in the Wilson Plot section was used here.

$$(UA)_{Overall} = \frac{Q_{H_2O}}{LMTD} \quad \textbf{[33]}$$

Q_{H2O} was used in this case because it is believed that the measurement of the H_2O heat transfer is more accurate than that of the CO_2. Now that both the $UA_{Overall}$ and U_{H2O} are

known, Equation 34 is solved. It should be noted here that both heat transfer areas are known constants.

$$\frac{1}{(UA)_{CO_2}} = \frac{1}{(UA)_{Overall}} - \frac{1}{(UA)_{H_2O}} \quad \textbf{[34]}$$

Finally, Equation 35 produces the results for the heat transfer coefficient of the CO_2.

$$U_{CO_2} = \frac{1}{\frac{1}{(UA)_{CO_2}} * A_{CO_2}} \quad \textbf{[35]}$$

The data received from Equation 35 was compared to correlations that are widely accepted. The Gnielinski correlation, Equation 1, was used to calculate a Nusselt number for the CO_2, which allows for the heat transfer coefficient to be determined from Equation 2. The Gnielinski correlation is valid for fluids that are in the range of 0.5<Pr<2,000 and 3,000<Re<5*10^6, of which all the tests are. Three different friction factors were used in solving the Gnielinski correlation, which were the Blasius, Haaland, and Colebrook & White correlations. (Ghajar) They can be observed in Table 10.

Table 10: Friction Factors Implemented

Friction Factor	Equation
Blasius	$f_{Bl} = 0.316 * \mathrm{Re}^{-1/4}$
Haaland	$\sqrt{1/f_{Ha}} = -1.8 * LOG\left[\frac{6.9}{\mathrm{Re}} + \left(\frac{\varepsilon/D}{3.7}\right)^{1.11}\right]$
Colebrook & White	$\sqrt{1/f_{Co}} = -2.0 * LOG\left[\frac{2.51}{\mathrm{Re}_{CO_2} * \sqrt{f_{Co}}} + \frac{\varepsilon/D}{3.71}\right]$

Figure 25 shows a graph of the measured heat transfer coefficient of CO_2 in the x-axis vs. the predicted heat transfer coefficient in the y-axis. Appendix K shows the EES code used

to calculate the expected heat transfer coefficient. As can be seen on the graph there are two lines, one showing 0% error and the other showing +75% error. Clearly, the measured data does not accurately correlate to the predicted values. The reasons for these deviations are discussed in the following Discussion section.

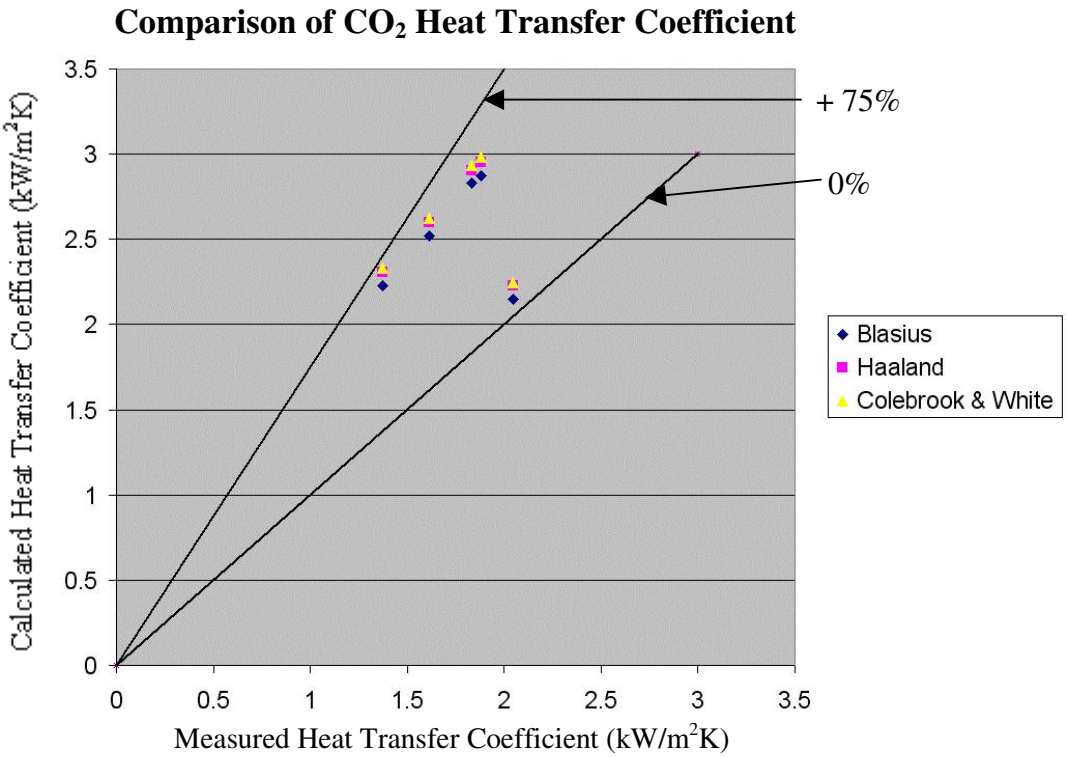

Figure 25: Comparison of Heat Transfer Coefficient

4.4.2 Pressure Drop

The pressure drop over the test section was measured by a GP:50 differential pressure transducer. This value was compared to a pressure drop that was calculated with two different friction factors, the Blasius, which is commonly used for pressure drop in smooth tubes with turbulent flow and the Colebrook & White, which is an implicit formula that

matches well with the Moody-Diagram. Both have been shown in Table 10. The pressure drop was calculated using the Darcy-Weisbach equation:

$$\Delta P = \left(\frac{\rho_{CO_2} * V_{CO_2}^2}{2} \right) * \left[\left(f * \frac{L}{D} \right) + K_L \right] \quad \textbf{[36]}$$

Where

ΔP = Pressure drop
ρ_{CO2} = Density of the refrigerant
V_{CO2} = Velocity of the refrigerant
f = Friction Factor, Blasius or Colebrook & White
L = Length of micro channel
D = Diameter of micro channel
K_L = Geometric minor losses due to bends, contractions and expansions

The results to Equation 36 are visualized in Figure 26 when it is assumed that the minor losses are negligible. Appendix L displays the EES code used to calculate the predicted pressure drop. The measured pressure drop is on the x-axis and the predicted pressure drop is on the y-axis. The two lines depict errors of 0% and minus 45%. Figure 26 shows that the predicted values for the pressure drop are consistently smaller than the measured values.

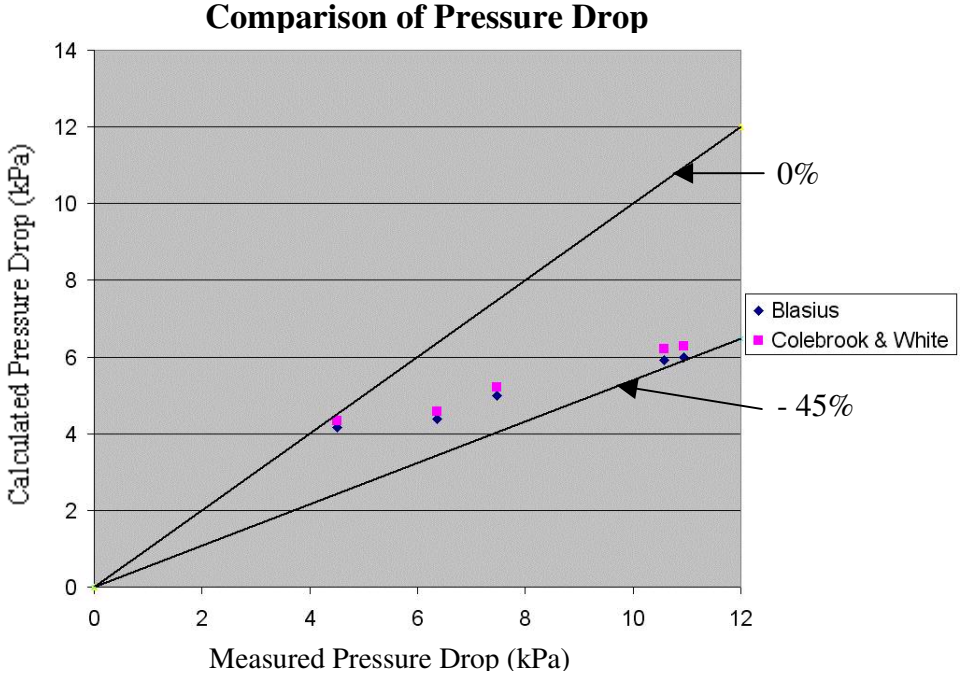

Figure 26: Comparison of Pressure Drop over Micro Channel

The minor losses that were perceived to be negligible were then incorporated into the pressure drop calculations. Figure 27 shows a top view of the test section and includes all points where minor losses occur between the differential pressure drop measurements. The largest minor losses are due to the tees in the flow and because the micro channel extends into the Al header, causing a reentrant entrance and exit.

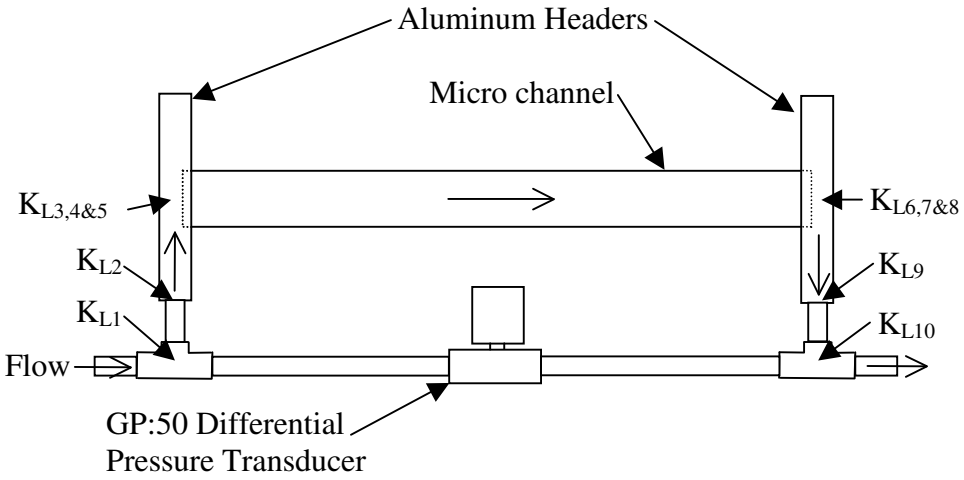

Figure 27: Schematic of Test Section for Points of Pressure Drop

All of the minor losses due to geometry are specified and their given values are shown in Table 11. The pressure drop analysis of Equation 36 was repeated; however this time the K_L value was 11.21 instead of zero. The results for this calculation can be observed in Figure 28. As expected the change was minimal; however it did reduce the error gap by 1%.

Table 11: Value for Geometric Losses

Loss	Geometric Effect	Value
K_{L1}	Tee	2.0
K_{L2}	Expansion	0.2319
K_{L3}	Tee	2.0
K_{L4}	Contraction	0.4
K_{L5}	Reentrant Entrance	0.8
K_{L6}	Tee	2.0
K_{L7}	Expansion	0.5234
K_{L8}	Reentrant Exit	1.0
K_{L9}	Contraction	0.25
K_{L10}	Tee	2.0
	Total:	11.21

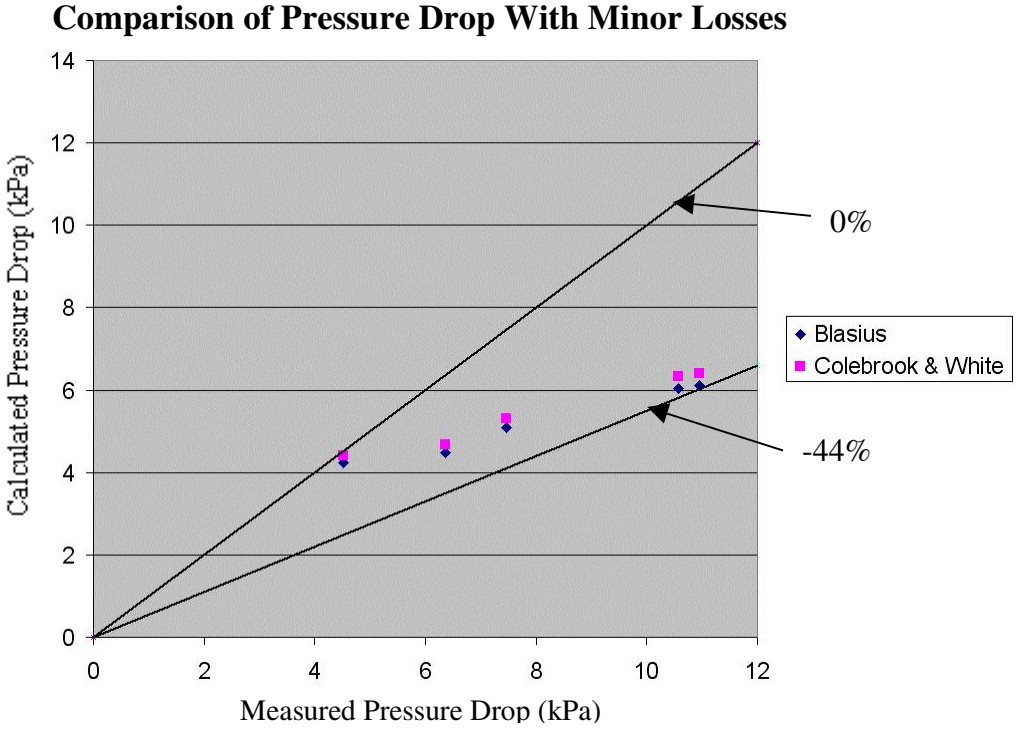

Figure 28: Comparison of Pressure Drop with Minor Losses over Micro Channel

4.5 Discussion

The system was successfully built and has produced data with minimal heat transfer balance error. Conversely, the test conditions were not exactly met due to a lack of control of the OCR level. Although controlling the OCR level was not mastered, the results to the

data received do follow trends currently accepted in the CO_2 field. Figure 25 shows that the measured heat transfer coefficients are significantly less than the predicted values. From past reports done, specifically Kuang et al., they found there is an increase in the heat transfer of CO_2 with minute amounts of oil. However, after a certain point, the oil negatively effects the heat transfer of the CO_2. Results from Kuang et al. can be observed that describe this phenomenon in Figure 29.

From the OCR calculations taken for each test for this project, it has been found that the OCR level ranged from 6.58 to 10.72%. Although the accuracy of these measurements is suspect due to the R-Series mass flow meter, it can be deduced that oil is circulating, even if the exact amount cannot be precisely calculated.

If the predicted heat transfer coefficients are taken as the base value (0 OCR%) in comparison to the measured value (varying OCR%), then the enhancement factor would be approximately 0.65, as seen in Figure 29. The exact values cannot be taken literally because of the uncertainty in the OCR measurement, but they do confirm the same trend shown in previous studies. Figure 29 shows that one of the five heat transfer coefficient measured is around 0.95, while the other four hover around 0.65. This individual test was run with a H_2O flow rate that was approximately 4.38 g/s in order to meet the heat flux condition, while the other four tests were run with a H_2O flow rate above 9.5 g/s in adherence to the discussion in the Lessons Learned section. This leads to the consideration that a change in the H_2O flow rate could drastically alter the result for the CO_2 heat

transfer coefficient, inferring that the Wilson Plot method should be repeated for accuracy validation.

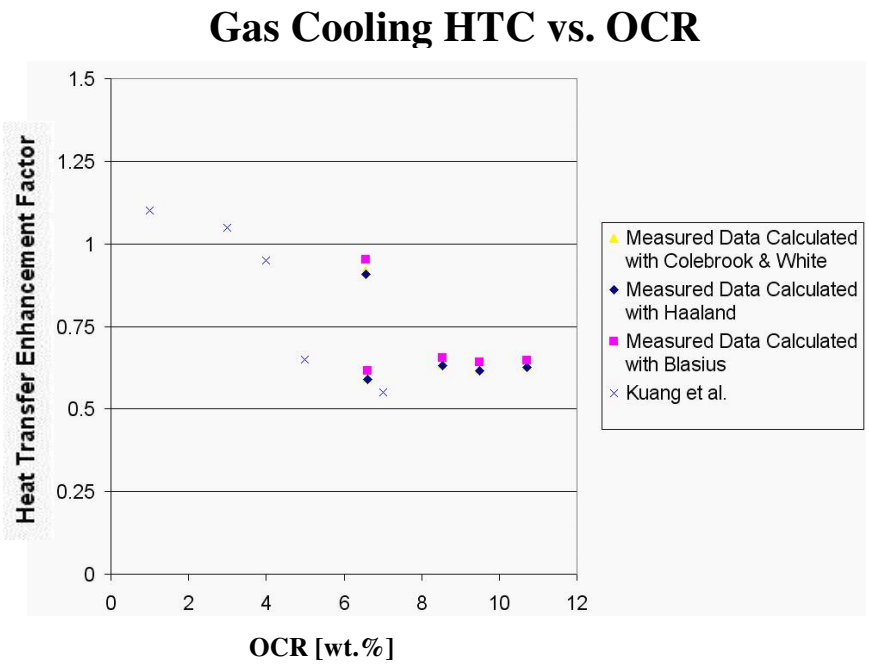

Figure 29: Heat Transfer Enhancement Factor vs. OCR

Similarly, Kuang et al. have shown what the effect of the OCR level has on the pressure drop over a micro channel. It has been deduced that an increase in the OCR level always results in an increase in the pressure drop, as shown in Figure 30. The driving and idling in the figure refer to the application of using CO_2 in an automobile.

Figure 30 shows the results if the predicted pressure drop is taken as a base point (0 %) and is compared with the measured value (varying OCR%). The data agrees with past results that the flow of oil with the CO_2 increases the pressure drop over the micro channel, although it shows an opposite trend. With the increase of OCR, the pressure ratio actually converges back to a ratio of 1.0. These five tests should not be directly compared to each

other because all five were taken at different pressure levels, ranging from 8 to 9.9 MPa, which can be observed in Table 9. A more appropriate discussion can be performed when a base line test with no OCR is compared to tests of the same test conditions except with the inclusion of varying OCR amounts. It is promising to see that the pressure drop is larger than the Darcy-Weisbach equation predicts, thus validating the notion that an inclusion of oil with CO_2 does increase the pressure drop. This is a phenomenon that needs to be included in heat exchanger design for CO_2 systems.

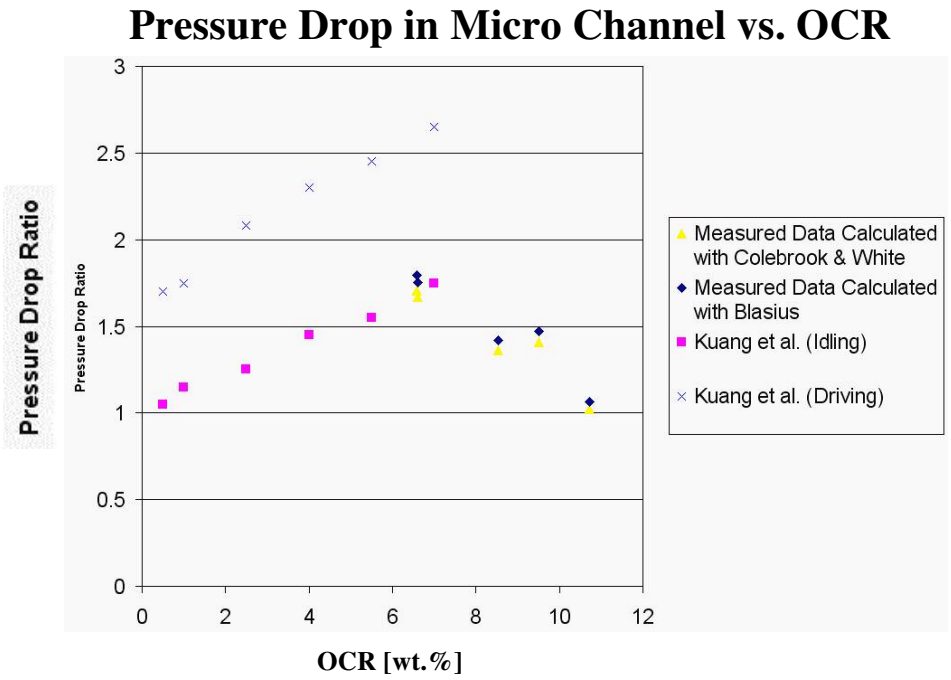

Figure 30: Pressure Drop Ratio vs. OCR

5 Conclusion

The goal of this project was to build a facility that could test the heat transfer coefficient and pressure drop effects of CO_2 flowing through a single, horizontal micro channel tube. Heat transfer was induced to occur over the micro channel by means of flowing H_2O in the opposing direction of the CO_2. A simple VCS was designed to generate the appropriate temperature and pressure test conditions needed. An expansion valve was used to obtain the specified CO_2 mass fluxes and alterations to the H_2O's temperature and flow rate allowed for all heat fluxes to be reached. A syringe pump was used to inject oil into the flow to reach the OCR wt.%'s, although the oil was never reduced to 0 wt.% under normal operating conditions. Therefore, the pump was never implemented. Five test conditions in the gas cooling range were achieved, although their calculated OCR levels were higher than was desired.

The results from this data produced reaffirming conclusions to other papers on oil flowing with CO_2. When the data points in this project were compared to common correlations as a baseline, it showed that the heat transfer coefficients of CO_2 were enhanced by a factor of approximately 0.65. Past projects, such as Kuang et al. showed a spike in the heat transfer coefficient for OCR levels below 3% and a decrease for in the heat transfer for OCR amounts higher than 3%. All of the OCR levels for the five data points taken were above 6% and confirmed this drop in heat transfer coefficient shown by Kuang. The data points also corroborated with Kuang's findings on the alteration of the pressure drop. Both Kuang and this project found that an inclusion of oil circulating with the CO_2 will cause an increase in the pressure drop.

6 Future Work

Although the experimental system has been built and tested, several tasks must be completed in order for future tests to be more accurate. The most important is to determine the reason for oil recirculation in the test section loop. There are two major issues to consider in regards to this dilemma. The first is the R-Series Micro Motion flow meter that is used in the CO_2 flow. The R-Series is the lowest model Micro Motion offers, although the low cost is an advantage it also has the lowest accuracy. This did not seem to be a setback when balancing heat transfers, however it is in regards to calculating an exact OCR amount. According to the uncertainty propagation feature in EES, the accuracy in the density readings of ± 10 kg/m^3 can lead to OCR measurements that are ± 5.0%. Since test conditions specify that tests be run at each integer from 0 through 5 percent, the R-Series flow meter is not efficient enough to produce valid data. The five tests that were run without injecting oil into the flow had an OCR level between 6.57% and 10.72%, but with the calculated propagation of ± 5.0% it is not known how much oil was actually recirculating.

Even if this error is reduced the problem still remains that some oil is recirculating. This problem can be addressed through two physical alternations. Either new separators that are not prototypes could be purchased and integrated into the system, or additional oil separators could be added to draw more oil out of the flowing CO_2. Next, the layout of the system itself could be altered. The compressor should be the lowest point in the system so that the oil can flow back into the compressor when the system is idle. Currently, the bottom half of the gas cooler and several pipes in both loops are the same height or lower

than the compressor. This will not be a minor task, especially since the compressor is placed upon a wooden frame and rubber plates to reduce vibrations; however, this would be very beneficial. In conjunction with the previous point, all of the components in the test section loop, particularly the test section itself should be placed higher than the VCS loop. Such an adjustment would limit the amount of oil entering the test section because the oil in the CO_2 would have to pass through three oil separators and overcome gravitational effects.

Another obstacle that needs to be overcome has to deal with the H_2O loop of the system. Since the test conditions call for CO_2 inlet temperatures that exceed 70°C and heat fluxes lower than 15 kW/m^2, the inlet temperature of the H_2O needs to be within 30 and 65°C. However, the H_2O chiller can only maintain a maximum recirculating temperature of 36°C. This was known before the project started and as stated, a screw plug immersion heater with a capacity of 500 W's was purchased to help heat up the H_2O. Unfortunately, when the immersion heater is turned on it increases the error in the heat transfer balance slightly. Currently, this is not a problem of high concern; however, the 500 Watt heater alone does not allow for the inlet H_2O temperature to reach a level needed to complete all of the test conditions. Another 500 Watt immersion screw plug heater is needed, as well as a variable autotransformer to control it. It is imperative that this device is grounded or it will drastically increase the error of the heat transfer balance by sending a current through the H_2O. The heat balance must also be checked to see if the addition of another immersion heater adds error to the heat transfer balance.

While it is believed that the Wilson Plot measurements were correctly implemented, if future heat transfer coefficients with 0% OCR do not exactly correlate to predictive models like the Gnielinski correlation, tests for the Wilson Plot method should be repeated to verify their accuracy. If oil is still circulating now, it definitely was when the Wilson Plot method was implemented causing errors in this data.

After the above is completed, the test matrix for gas cooling, including all of the conditions in Table 2 needs to be completed and analyzed. Additional conditions are hoped to be completed for convective boiling as well. This would require the system to be changed so that the inlet CO_2 into the test section comes before the evaporator, since it is the lowest temperature location of the VCS. There are three test sections that have been dip brazed by Ridge Engineering Co. that can be implemented in these tests.

APPENDIX A: Dorin Two Stage CO_2 Compressor

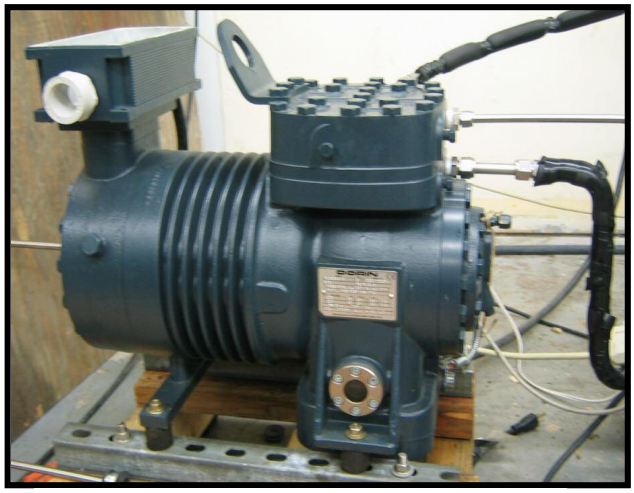

Figure 31: Dorin Two-Stage

APPENDIX B: Parker CO_2 Oil Separator

Figure 32: Parker CO_2 Oil Separator

APPENDIX C: Sensing Devinces, Inc. RTD

Figure 33: Sensing Devices, Inc. RTD

The actual probe of extends six inches past where the 1/8" Swagelok Nut and Ferrule is attached.

APPENDIX D: Setra Systems In-Stream Pressure Transducer

Figure 34: Setra In-Stream Pressure Transducer

APPENDIX E: GP:50 Differential Pressure Transducer

Figure 35: GP:50 Differential Pressure Transducer

APPENDIX F: Micro Motions Coriolis Mass Flow Meter

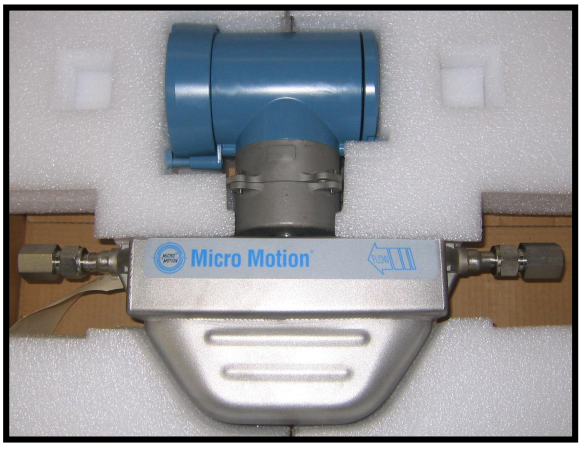

Figure 36: Micro Motion Mass Flow Meter Model R250P

APPENDIX G: Sponsler Co., Inc. Volume Flow Meter

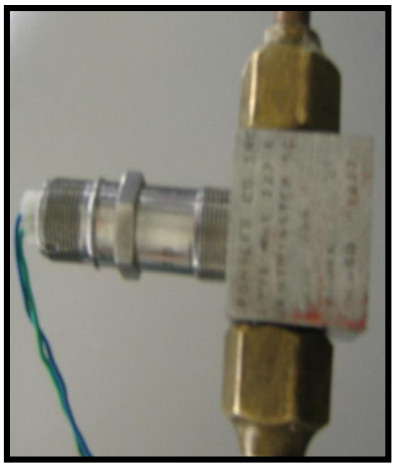

Figure 37: Sponsler Co., Inc. Turbine Volume Flow Meter

APPENDIX H: National Instruments Data Acquisition Modules

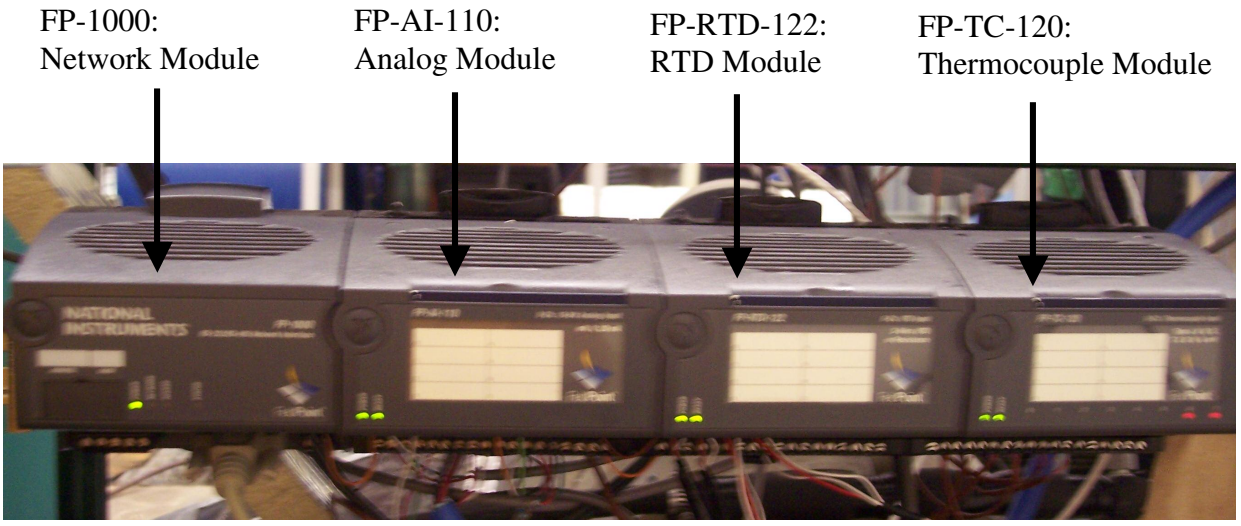

Figure 38: National Instrument Data Acquisition Modules

APPENDIX I: NesLab HX-75 Re-circulating H_2O Chiller

Figure 39: NesLab HX-75 H_2O Chiller

The H_2O chiller is fully operational in this picture. Both the re-circulating inlet and outlets are labeled. The tap H_2O inlet and outlet are not visible in this picture; they are attached to the back. A CO_2 measuring device can also be seen on the H_2O chiller for safety reasons.

APPENDIX J: Screw Plug Immersion Heater, 500 Watts

Figure 40: Screw Plug Immersion Heater

APPENDIX K: Code for Predicted Heat Transfer Coefficient

```
Ao=0.018; {m}          Bo=0.004; {m}                {Dimensions of H2O Opening}
Ai=0.016053; {m}       Bi=0.001994; {m}             {Outer Dimensions of Micro channel}
Di=0.001056; {m}  n=10; L=0.470; {m}                {Characteristics of Micro channel}
L_h2o=0.5904;          {m}                          {Length H2O flows over Micro channel}
D_header=0.00635; {m}  L_header=0.1524; {m}         {Dimensions of Al Header}
D_steel=0.004572  {m}                               {Diameter of Steel Tubing}
Dh_h2o=(4*(XSectAreao))/(2*(Ai+Bi)+2*(Ao+Bo))  {m}  {Hydraulic Diameter of H2O}
Areai=pi*Di*n*L  {m^2}                              {CO2 HT area}
Areaio=L*2*(Ai+Bi)  {m^2}                           {H2O HT area}
Areao=L*2*(Ao+Bo)  {m^2}                            {Total cross sectional area}
XSectAreai1=pi*((Di/2)^2)  {m^2}                    {Cross Sectional Area for individual port}
XSectAreao=(Ao*Bo)-(Ai*Bi)  {m^2}                   {Cross Sectional Area for H2O}
XSectArea_Header=pi*((D_header/2)^2)  {m^2}         {Cross Sectional Area for Al Header}
XSectArea_steel = pi*((D_steel/2)^2)  {m^2}         {Cross Sectional Area for Steel Tubing}
Ratio_Area = (XSectAreai1*n) / XSectArea_Header     {Area Ratio Header to Micro Channel}
Ratio_Area2 = XSectArea_steel / XSectArea_Header    {Area Ratio Header to Steel Tubing}

G_co2=392.336  {kg/s*m^2}                           {Mass flow flux}
T1_co2=69.315  {C}                                  {CO2 Inlet Temperature}
T2_co2=48.481  {C}                                  {CO2 Outlet Temperature}
Tave_co2 = (T1_co2+T2_co2)/2  {C}                   {CO2 Average Temperature}
Pin_co2=9876.515  {kPa}                             {CO2 Inlet Pressure}
PD_co2=4.514  {kPa}                                 {CO2 Differential Pressure}
Pout_co2= Pin_co2 - PD_co2  {kPa}                   {CO2 Outlet Pressure}
Pave_co2 = (Pin_co2+Pout_co2)/2  {kPa}              {CO2 Average Pressure}

{CO2  Viscosity}
mu_co2=viscosity(CARBONDIOXIDE,T=Tave_co2,P=Pave_co2)  {kg/m*s}
{CO2 Outlet Density}
rho_co2=density(CARBONDIOXIDE,T=T2_co2,P=Pout_co2)  {kg/m^3}
{CO2 Average Density}
rho_co2_ave=density(CARBONDIOXIDE,T=Tave_co2,P=Pave_co2)  {kg/m^3}
{CO2 Specific Heat}
cp_co2=cp(CARBONDIOXIDE,T=Tave_co2,P=Pave_co2)  {kJ/kg*K}
{CO2 Thermal Conductivity}
k_co2=conductivity(CARBONDIOXIDE,T=Tave_co2,P=Pave_co2)*(10^(-3))  {kW/m*K}
{CO2 Reynolds Number}
Re_co2=G_co2*Di/mu_co2
{CO2 Prandtl Number}
Pr_co2=cp_co2*mu_co2/k_co2;
{CO2 Mass Flow Rate}
MASSflowRATE_co2=G_co2*XSectAreai1*n  {kg/s}
```

{Blasius Friction factor}
f_co2_Bl =0.316*Re_co2^(-0.25)

{Gnielinski Correlation with Blasius Friction factor}

Nu_co2_Bl=((f_co2_Bl/8)*(Re_co2-1000)*Pr_co2)/(1+12.7*(f_co2_Bl/8)^(1/2)*(Pr_co2^(2/3)-1))

{CO2 Heat Transfer Coefficient with Blasius Friction factor}

h_co2_Bl=k_co2*Nu_co2_Bl/Di {kW/K*m^2}

{Haaland Friction factor}
epsilon=1.0*10^(-6) {m}
sqrt(1/f_co2_Ha) = -1.8*log10((6.9/Re_co2)+(((epsilon/Di)/3.7)^1.11))

{Gnielinski Correlation with Haaland Friction factor}
Nu_co2_Ha=((f_co2_Ha/8)*(Re_co2-1000)*Pr_co2)/(1+12.7*(f_co2_Ha/8)^(1/2)*(Pr_co2^(2/3)-1))

{CO2 Heat Transfer Coefficient with Haaland Friction factor}
h_co2_Ha=k_co2*Nu_co2_Ha/Di {kW/K*m^2}

{Colebrook & White Friction Factor}
1/sqrt(f_co2_Co)=-2.0*log10((2.51/(Re_co2*sqrt(f_co2_Co)))+(epsilon/Di)/3.71)

{Gnielinski Correlation with Colebrook & White Friction Factor}
Nu_co2_Co=((f_co2_Co/8)*(Re_co2-1000)*Pr_co2)/(1+12.7*(f_co2_Co/8)^(1/2)*(Pr_co2^(2/3)-1))

{CO2 Heat Transfer Coefficent with Colebrook & White Friction factor}
h_co2_Co=k_co2*Nu_co2_Co/Di {kW/K*m^2}

APPENDIX L: Code for Predicted Pressure Drop*

```
g = 9.8  {m/s^2}                                        {Gravity}
V_co2 = G_co2 / rho_co2_ave  {m/s}                      {CO2 Velocity}

{Minor Losses}
K_L_Tees = 2.0
K_L_Entrance = 0.8
K_L_Exit = 1.0
L_channel = 0.6
K_L_Ratio_Area_cont = 0.4
K_L_Ratio_Area_exp = ((1-(XSectAreai1*n) / XSectArea_Header))^2
K_L_Ratio_Area_cont2 = 0.25
K_L_Ratio_Area_exp2 = ((1-( XSectArea_steel / XSectArea_Header)))^2
K_L_Sum = 4*K_L_Tees + K_L_Entrance + K_L_Exit + K_L_Ratio_Area_cont
+K_L_Ratio_Area_exp +K_L_Ratio_Area_cont2+K_L_Ratio_Area_exp2

{Pressure Drop with Minor Losses and Colebrook & White Friction Factor}
Delta_P_Co / (rho_co2_ave) = f_co2_Co * ((L_channel/(Di)) +K_L_Sum) * ((V_co2^2)/(2))  {Pa}

{Pressure Drop with Minor Losses and BlasiusFriction Factor}
Delta_P_Bl / (rho_co2_ave) = f_co2_Bl * ((L_channel/(Di)) +K_L_Sum) * ((V_co2^2)/(2))  {Pa}

{Pressure Drop without Minor Losses and Colebrook & White Friction Factor}
Delta_P_Co_NOK = f_co2_Co * (L_channel/(Di))* ((V_co2^2)*rho_co2_ave)/2  {Pa}

{Pressure Drop without Minor Losses and BlasiusFriction Factor}
Delta_P_Bl_NOK = f_co2_Bl * (L_channel/Di)* ((V_co2^2)*rho_co2_ave)/2  {Pa}
```

*This code incorporates variables that were calculated in the EES heat transfer coefficient code, Appendix K.

References:

ASHRAE Handbook of Fundamentals, SI Edition 2001, Chapter 3, pp. 3.1-3.12.

ASHRAE Handbook of Fundamentals, SI Edition 2001, Chapter 35, pp. 35.1-34.3.

Akers, W.W., H.A. Deans and O.K. Crosser, 1959. "Condensing Heat Transfer within Horizontal Tubes," Chemical Engineering Progress Symposium Series 55(29): 171-176.

Bredesen, A.M., Hafner, A., Pettersen, J., Neksa, P., Aflekt, K., 1997, Heat Transfer and Pressure Drop for In-tube Evaporation of CO_2. *Proceedings IIR Conference: Heat Transfer Issues in 'Natural' Refrigerants*, p. 35-49.

Drees, D., Fahl, J. and J. Hinrichs, 2002, "Effect of CO_2 on Lubricating Properties of Polyesters and Polyalkylene Glycols," *Proceedings of the 13th International Colloquium Tribology, Esslingen*, Vol 1, p 425, January 15 – 17.

Emerson Process Management, March 2004, Product Data Sheet: Micro Motion R-Series Mass and Volume Flowmeter with MVD Technology. http://www.documentation.frco.com/groups/public_public_mmisami/documents/data_sheets/ps-00363.pdf, March 13th, 2005.

Gabola, Salvatore, 2003. "Refrigerants, Naturally." The Coca-Cola Company Alternative Refrigeration Backgrounder. http://www.refrigerantsnaturally.com/doc/The%20Coca-Cola%20Company%20backgrounder.pdf. March 22nd, 2005.

Ghajar A.T., Asadi A., 1986: Improved Forced Convective Heat Transfer Correlation for Liquids in the Near Critical Region. AIAA Journal Vol. 24, No. 12, p. 2030-2037.

Gnielinski, V., 1973. New Equations for Heat and Mass Transfer in Turbulent Pipe and Channel Flow, *International Chemical Eng*. Vol. 16, p. 359-368.

Haaland, S.E., 1983, Simple and Explicit for the Friction Factor in Turbulent Pipe Flow. *Journal Fluids Eng*., March, p. 89-90.

Halozan, H., Ebner, T., Lawatsch, H., September 1994, "Propane and CO_2 Two 'Natural' Alternatives," *IIR*, p. 329-336.

Hwang, Y., Kim, B.H., Radermacher, R., 1997, "Boiling Heat Transfer Correlation for Carbon Dioxide," Heat Transfer Issues in 'Natural' Refrigerants, Vol. 1, University of Maryland, USA.

Kuang, G., Ohadi, M., Zhao, Y., 2004, "Experimental Study on Gas Cooling Heat Transfer for Supercritical CO_2 in Microchannels," *Second International Conference on Microchannels and Minichannels*, p. 325-332, June 17-19.

Li, H., and Rajewski, T.E., 2000, "Experimental Study of Lubricant Candidates for the CO2 Refrigeration System," *Proceedings of the 4th IIR-Gustav Lorentzen Conference on Natural Working Fluids at Purdue*, p. 409, July 25-28.

Lorentzen, G., 1995: The Use of Natural Refrigerants: A Complete Solution to the CFC/HCFC Predicament. *International Journal of Refrigeration*. Vol. 18, No. 3, p. 190-197.

Munson, Bruce, Young, Donald, Okiishi, Theodore, 2002. Fundamentals of Fluid Mechanics, 4th Edition. Ames, Iowa. John Wiley & Sons, Inc., p. 480-489.

Neksa, P., Pettersen, J., Skaugen, G., 2001, "Heat Transfer and Pressure Drop of Evaporating CO_2 in Microchannels and System Design Implications of Critical Heat Flux Conditions," *ASME International Mechanical Engineering Congress and Exposition,* Nov. 11-16. New York, NY.

Pettersen, J., Hafner, A., Skaugen, G., Rekstad, H., 1998, "Development of Compact Heat Exchangers for CO_2 Air-Conditioning Systems," *International Journal of Refrigeration* Vol. 21, No. 3, p. 180-193.

Pettersen, J., Rieberer, R., Munkejord, S. T., February 2000, "Heat Transfer and Pressure Drop for Flow of Supercritcal and Subcritical CO_2 in Microchannel Tubes," SINTEF Energy Research / Norwegian University of Science and Technology.

Rieberer, Rene, 1999, CO_2 Properties, SINTEF Energy Research, N-7465 Trondheim.

Shah, M.M., 1979, "A General Correlation for Heat Transfer During Film Condensation Inside Pipes," Int. J. Heat Mass Transfer 22: 547556.

Seeton, C., Fahl, J. and Henderson, D., 2000, "Solubility, Viscosity, Boundary Lubrication and Miscibility of CO2 and Synthetic Lubricants," *Proceedings of the 4th IIR-Gustav Lorentzen Conference on Natural Working Fluids at Purdue*, p. 417, July 25-28.

Tran, T.N., M.W. Wambsganns and D.M. France, 1996, "Small Circular and Rectangular Channel Boiling with Two Refrigerants," Int. J. Multiphase Flow 22(3): 485-498.

Yang, C.Y. and R.L. Webb, 1997, "A Predictive Model for Condensation in Small Hydraulic Diameter Tubes Having Axial Mico-fins." ASME J. Heat Transfer 119: 776-782.

Zhao, Y., Ohadi, M., Dessiatoun, S., Molki, M., Darabi, J., 1999, "Forced Convection Boiling Heat Transfer of CO_2 in Horizontal Tubes," *Proceedings of the 5th ASME/JSME Joint Thermal Engineering Conference*, March 15-19.